Published in Materials Horizons, 13 (2026) 1165

Carbon nanotube-enabled coatings for advanced anti-icing and deicing applications

Monika Tarnowska[1], Artur P. Terzyk[2], Joanna Kujawa[2], Sławomir Boncel[1,3,4,*]

[1]Silesian University of Technology, Faculty of Chemistry, Department of Organic Chemistry, Bioorganic Chemistry and Biotechnology, NanoCarbon Group, 4 Bolesława Krzywoustego St., 44-100 Gliwice, Poland

[2]Nicolaus Copernicus University in Toruń, Department of Chemistry, Physicochemistry of Carbon Materials Research Group, 7 Gagarin St., 87-100 Toruń, Poland

[3]Silesian University of Technology, Centre for Organic and Nanohybrid Electronics (CONE), 22B Stanisława Konarskiego St., 44-100 Gliwice, Poland

[4]NanoCarbonGroup.com Co. Ltd., 7 Ks. Marcina Strzody St., 44-100 Gliwice, Poland

*Corresponding author: slawomir.boncel@polsl.pl

TOC

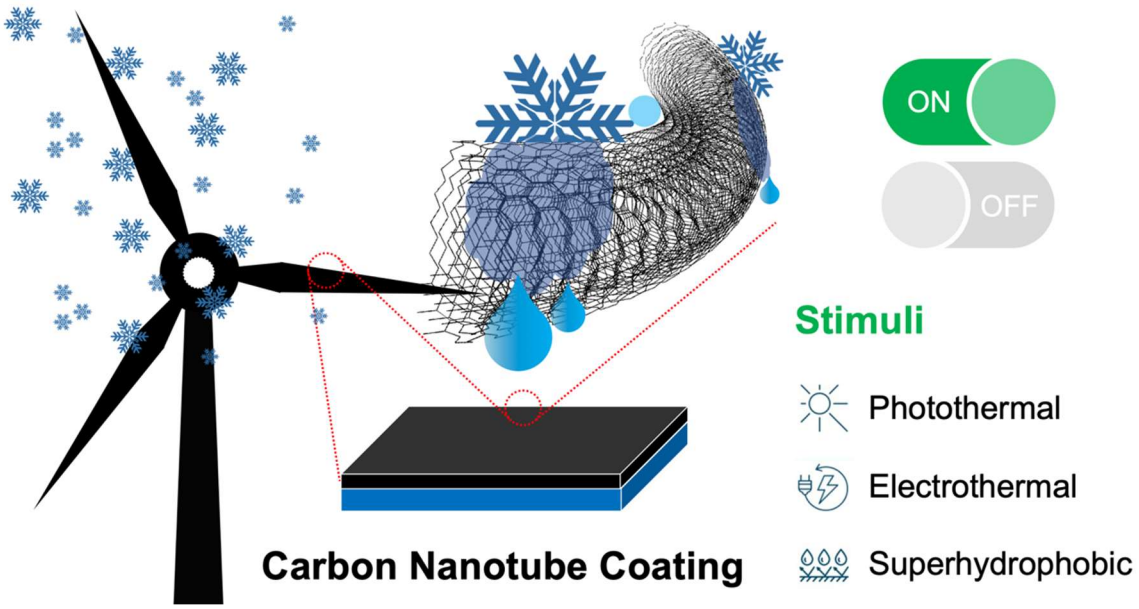

This review charts recent advances in carbon nanotube-based coatings for ice mitigation, revealing how surface morphology and physicochemistry, interpreted through Hansen Solubility Parameters, guides the scalable design of durable, climate-resilient anti-icing technologies integrating passive and active functionalities.

Abstract

Ice accumulation presents persistent challenges across critical infrastructure sectors, including aviation, energy transmission, transportation, and telecommunications. With the advancement of nanomaterials, carbon nanotubes (CNTs) have emerged as powerful components for the design of high-performance anti-icing and deicing coatings. Owing to their exceptional thermal, electrical, and surface properties, CNTs enable both passive (*e.g.*, superhydrophobic) and active (*e.g.*, photothermal, electrothermal) strategies for ice mitigation. This review critically examines the integration of pristine and chemically modified CNTs into functional coatings, highlighting synthesis approaches, surface engineering, performance metrics, and operational mechanisms – reported from 2016 to 2025. Particular emphasis is placed on the correlation between coating efficacy and the physicochemical characteristics of CNT surfaces, interpreted through the framework of Hansen Solubility Parameters (HSPs) as a predictive tool for CNT–matrix compatibility and icephobic performance. By mapping structure–function relationships and identifying synergistic design strategies, this work provides a comprehensive perspective on the future development of scalable, durable, and climate-resilient CNT-based anti-icing and deicing technologies.

1. Introduction

Ice accumulation is a growing concern in industrial settings, affecting aircraft, power lines, roads, telecommunications facilities, and wind turbine blades.[1] For instance, in wind farms, strong centrifugal forces on the blades may throw the assembled ice at high speeds. Moreover, the uneven ice cover across the three blades can lead to an imbalanced rotation and cause extra stress on the hub.[2] In aviation, ice accretion seriously threatens safety due to weight gain, shape changes in the aerodynamic profile, or fixation of moving parts.[3] Additionally, ice cover on the radome surface (a protective, weather-resistant structure shielding a radar antenna from environmental elements) may cause radio-frequency interference, preventing efficient communication at high altitude.[4,5]

Applied strategies focus on preventing ice formation (anti-icing) and removing existing ice (deicing). Some methods may operate without energy input (passive), making them efficient for long-term use, while others require energy (active) and are suitable for rapid response in severe conditions.[6] They can be grouped into categories: electrothermal, mechanical, photothermal, chemical methods, vapor, and microwave heating; surface modification, such as hydrophobization; and slippery systems[6–9] (**Fig. 1**). While coatings offer passive operation,[6,10,11] durability,[12] cost-effectiveness, safety enhancements, environmental benefits,[7] versatility,[13] and efficiency in ice management,[14] they are an interesting solution for anti-icing and de-icing applications. Among the strategies discussed, all except mechanical methods and vapor heating can be implemented as coatings.[6,7,12]

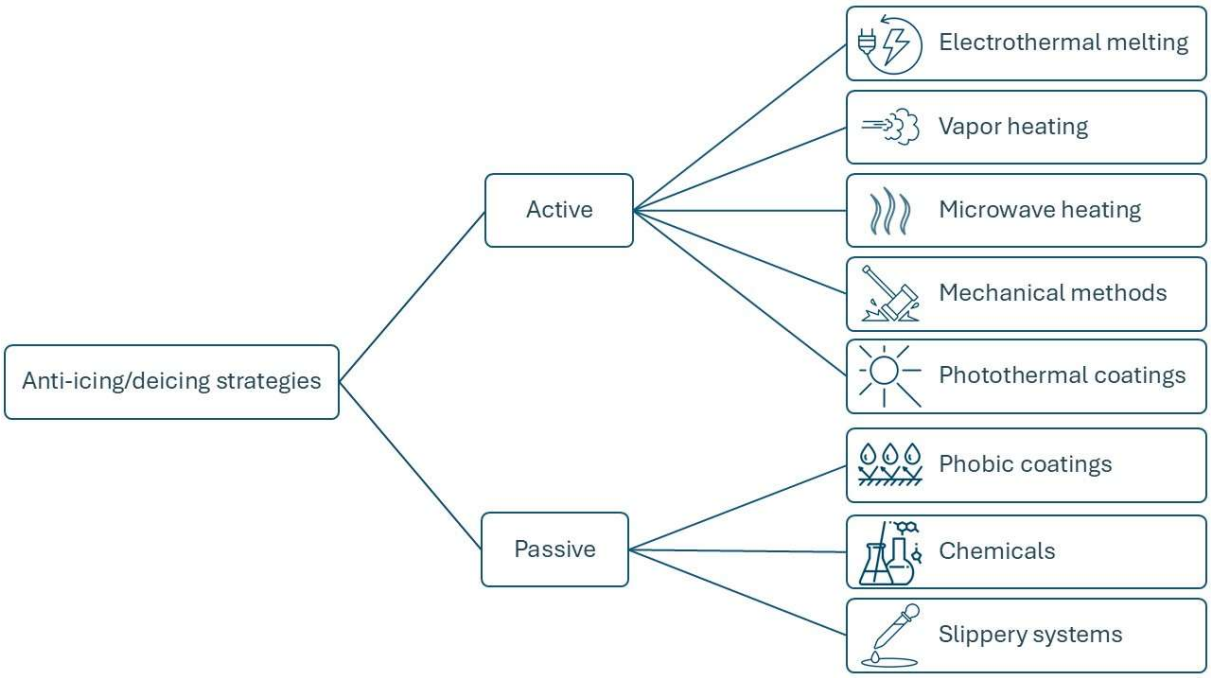

Fig. 1. Categories of anti-icing and deicing methods.

Carbon nanotubes (CNTs), with their unique combination of excellent physical properties (**Table 1**), emerge as promising candidates for application in coatings that prevent or remove ice. Due to their nanostructured surface and low surface energy, coatings prepared from CNTs demonstrate hydrophobic or even superhydrophobic properties. Moreover, they can be functionalized[15] or combined with other materials (*e.g.*, polymers, fluorides) to achieve a static water contact angle (WCA) greater than 150°, enabling water repellency[16] and lowering ice adhesion.[17] CNTs have exceptional thermal conductivity, enabling rapid heat transfer for active de-icing.[18,19] They possess high electrical conductivity, allowing them to function as conductive coatings for Joule heating.[20–22] High tensile strength and Young's modulus ensure that CNT-based coatings remain durable under mechanical stress, abrasion, and environmental exposure.[2,20] Owing to their ability to absorb light across a broad spectrum and convert it into heat *via* the photothermal effect, CNTs support active de-icing without external power sources in sunlight-exposed environments.[20] On the other hand, it is important to emphasize the critical distinction between the intrinsic properties (mechanical, thermal, electrical, *etc.*) of individual

CNTs and those of bulk or 3D CNT networks. In these assemblies, interfacial contact resistance and weak van der Waals interactions significantly diminish the overall effective properties. For instance, although individual CNTs are known to possess extremely high thermal conductivity, the presence of junctions, entanglements, and imperfect contacts within 3D networks leads to considerable thermal losses, even up to few orders of magnitude.

Table 1 Physical properties of *individual* single-walled CNTs (SWCNTs) and multi-walled CNTs (MWCNTs).

Property	SWCNTs	MWCNTs
WCA[a]	131.6° [23]	160° [24]
Thermal conductivity	6000 $W \cdot m^{-1} \cdot K^{-1}$ [18]	3000 $W \cdot m^{-1} \cdot K^{-1}$ [18]
Electrical conductivity	10^6 S/m [20]	$5 \cdot 10^3$ S/m [25]
Tensile strength[b]	25–66 GPa [26]	63 GPa [27]
Young's modulus[b]	1.0 TPa [20]	1.0–1.2 TPa [20]
Light absorbance[a]	200 nm – 200 μm [20]	350 nm – 17 μm [28]

[a] – recorded for an isotropic only-nanotube film; [b] – upon elongation

This review presents a comprehensive analysis of the current literature on pristine and chemically modified carbon nanotubes as high-performance nanofillers in engineered coatings for anti-icing and deicing applications. It examines the formulation strategies, fabrication methods of CNT-based nanocomposites, and the experimental approaches used to assess ice-repellent performance. The discussion encompasses findings reported from 2016 to 2025.

2. How to prepare an effective anti-icing/deicing coating?

An analysis of literature (**Fig. 2**) reveals that phobic surface modification (hydrophobic, superhydrophobic, or amphiphobic) is the most prevalent ice-repellent strategy employed in CNT-based coatings. This dominance can be attributed to the inherent hydrophobicity and high surface roughness imparted by CNTs. Photothermal approaches, which utilize the excellent light-to-heat conversion efficiency of CNTs, facilitate rapid surface heating and ice melting. Electrothermal strategies are also frequent but may be limited by energy requirements and integration challenges. Lubricated surfaces and microwave-heated systems are relatively uncommon, likely due to long-term stability and implementation complexity concerns.

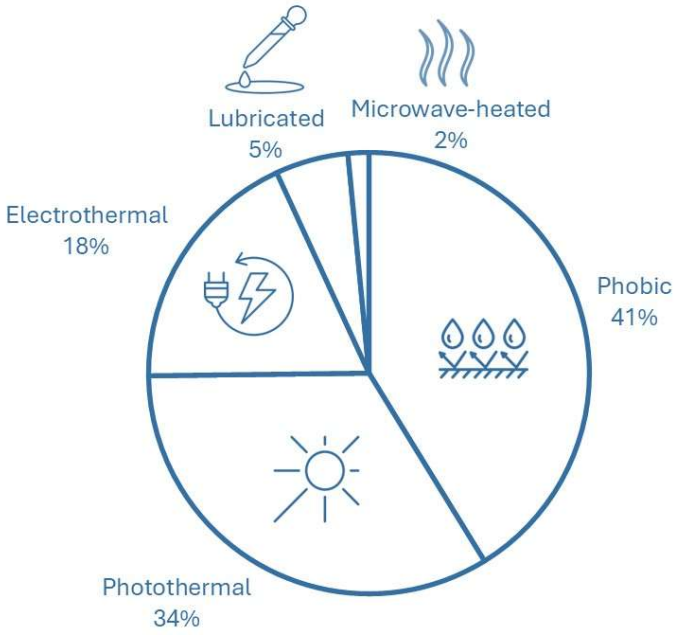

Fig. 2. The graph presenting the frequency of ice-prevention strategy occurrence in reviewed research articles.

The general process of preparing a CNT-based ice-proof coating is presented in **Fig. 3**. Regardless of the strategy employed, the first step involves considering the chemical composition. In the basic case, the coating may contain only pristine or modified CNTs, solvent,

and dispersants such as sodium dodecyl benzene sulfonate,[4,5] poly(*N*-vinylpyrrolidone) (PVP),[29] cetyltrimethylammonium bromide,[30] or sodium dodecyl sulfate.[31] The most commonly used solvents were water,[4,5,32–36] *n*-hexane,[37–40] ethanol,[32,34,41–49] xylene,[50–53] tetrahydrofuran (THF),[54] ethyl acetate,[55–58] and the mixture of acetone and toluene.[59,60] To improve adhesion strength, a wide range of binders have been found useful, *e.g.*, silicone resins,[29,37,45,61,62] epoxy resins,[30,34,36,41,47,56,62–66] polydimethylsiloxane (PDMS)[29,38,39,48,50,53,57,58,67–74], polyurethanes (PUs),[31,51,52,59,75] acrylic resins,[32,76,77] fluoro-modified polymers.[33,44,55,57,60,78–82] It is worth mentioning that Wang *et al.* developed a custom-made plant-originated binder, epoxidized soybean oil, with a specially synthesized curing agent through the condensation of vanillin and 1,10-diaminodecane.[83] Micro- and nanosized powders were predominantly added to facilitate the creation of a rough hierarchical structured surface or improve electroconductivity or photothermal effect. Additives that were applied are silicon carbide,[42,62,84] carbon nanofibers (CNFs),[43] graphene,[68,85] reduced graphene oxide (rGO),[86] silica nanoparticles,[29,35,85] carbon powder,[54,73] zinc oxide,[38] zinc acetate microparticles,[46] iron powder,[78] graphite powder,[57,71] or titanium nitride.[57] Preparation of stable dispersions was conducted by ultrasonication,[4,5,29–31,33,35–42,44,46,47,51,52,57,65,66,69,70,73,75,81,82,85–90] mechanical stirring,[30–34,45,48,49,51,53,54,57,58,60–64,66,67,69,73,80,82,84,85,91,92] or grinding.[32,55,59,60,79]

In the coating stage, due to the wide range of potential applications, many substrates were examined, such as glass,[4,5,34–37,39,44–46,50,53,57,60–62,68,71,74,76,78,83,86,89] poly(ethylene terephthalate) (PET),[88] a mixture of poly(ethylene terephthalate) and polyamide non-woven textile substrate,[93] 'ethylene vinyl acetate' (poly(ethylene-*co*-vinyl acetate),[42] steel,[41,62,87] tin,[50,55,79] aluminum,[29,32,46,53,59,62,63,70,81–83,91] asphalt,[56,61,76–78,80,84] polycarbonate,[85] glass fiber reinforced plastic,[31,43,46,51,52,94] self-healable poly(urea–urethane),[54] epoxy,[38,47,49] silicone rubber,[38,44,69] nylon,[38] poly(methyl methacrylate),[38] polytetrafluoroethylene (PTFE),[38,46] insulating paper,[38] wood,[46,90] concrete,[33,64–67,73,91,95] cellulose acetate,[40] PU foam,[48] aramid paper,[58] copper,[92,96]

paper,[62] fiberglass cloth,[75] and cotton.[72] Coating methods were primarily dedicated to conveniently covering large areas, which is why spray coating was the most common method.[5,29,31–36,38,41,42,44–49,51,52,54,56,58–67,69–71,73,74,78,80,82–84,86,89–92,94–96] Nevertheless, other industrial and laboratory techniques were applied, such as: dripping,[37,43,85] brushing,[64] rotary screen printing,[93] milling between two samples,[87] spin coating,[4,39] scraping,[57,76] slot-die coating,[88] sprinkling,[77] filtration under vacuum,[40] or immersing.[72,91]

In some cases, a topcoat layer was added to improve the efficiency of proposed coatings. This additional preservation can be divided into two categories: lubrication, in which oily substances are applied to the surface, and insulation, a topcoat layer improving hydrophobicity. Applied lubricants were: paraffin,[39,71] paraffin wax,[40] silicone oil,[53,91] coconut wax and coconut oil,[75] *n*-tetradecane,[65,96] perfluorodecalin,[87] while in top coatings were used: 1*H*,1*H*,2*H*,2*H*-perfluorodecyltrimethoxysilane,[44] PDMS,[48,72] hollow glass microsphere dispersed in epoxy resin,[71] or polypyrrole dispersed in PDMS.[70] Fan *et al.* developed a complex superhydrophobic topcoat based on epoxy resin, kaolin clay, silica nanoparticles, and hexadecyltrimethoxysilane.[64] A specific example of additional surface treatment was presented by Lin *et al.*, who applied laser etching to peel the pure resin film from the top of the coating.[32]

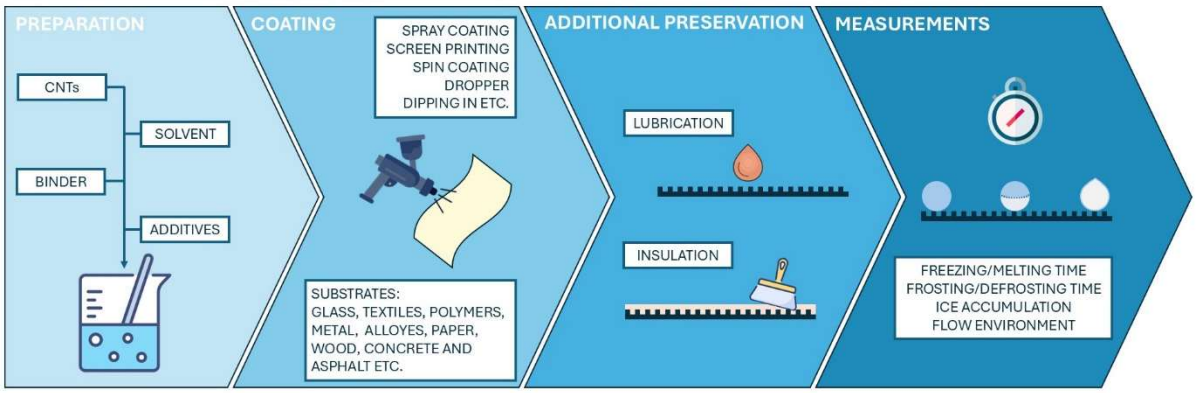

Fig. 3. Process of preparation and examination of ice-repellent coating.

3. How to prove anti-icing/deicing ability?

3.1. Freezing time

As there are many ways to prevent ice formation, methods of assessing their effectiveness are also diverse. The most common approach is to measure the time it takes for a droplet to freeze. The freezing time is defined as the duration from when the droplet completely changes from the liquid to the solid phase. During freezing, droplet shape changes, creating a sharp top similar to a hazelnut (**Fig. 4**).[60] Mostly, it is about recording or observing the process of the droplet freezing in a climate chamber,[32,42,46,54,64,76,85] or a lab refrigerator.[45,77] Droplet freezing on the examined surface may also be enabled by attachment to a thermal-conductive plate cooled by a cryogenic circulator,[59,60] or a Peltier cooling platform.[38] The process may be conducted with or without an external source of power, such as solar or electric, depending on the anti-icing strategy.[60]

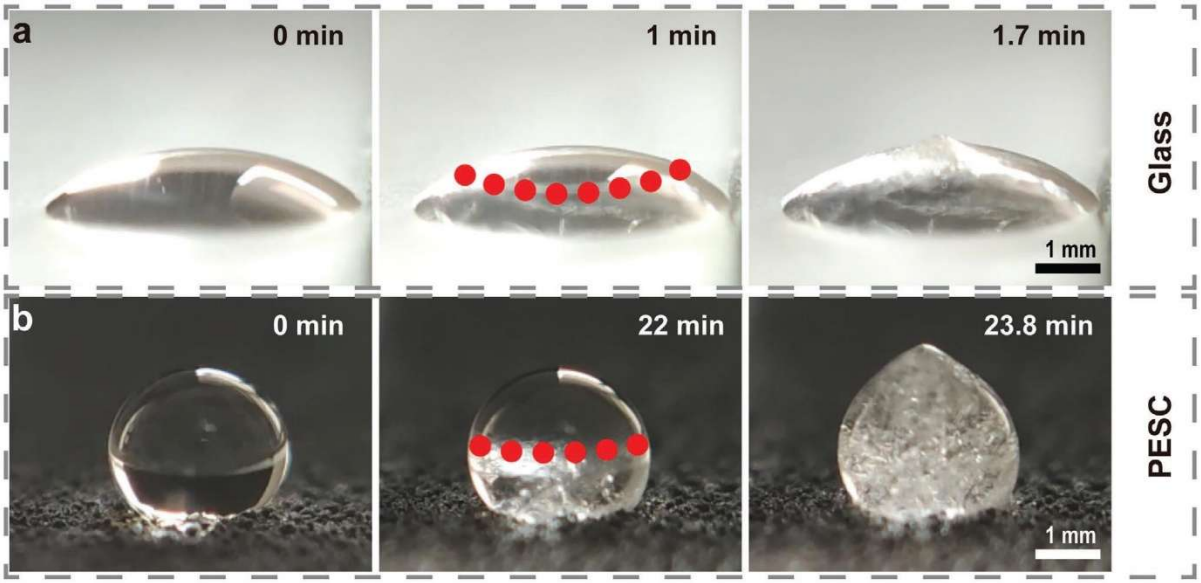

Fig. 4. Droplet freezing process on glass (a) and superhydrophobic surface (b). Reproduced with permission from ref.[60] Copyright 2021 Wiley.

3.2. Melting time

For indicating droplet melting time, the process is usually recorded in a climate chamber with power supply gained by irradiation under near-infrared (NIR) laser (**Fig. 5**),[42,54,67] Xenon lamp on the power level equals 1 sun (standard solar illumination of 1000 W m^{-2} under the AM1.5G spectrum, *i.e.*, sunlight when the sun is at a 48.2° angle from vertical meaning it passes through 1.5 times the thickness of the atmosphere; this arrangement simulates average terrestrial sunlight conditions, including both direct and diffuse components),[30,33,47,59,60] solar light simulator,[32,46,53] or direct current voltage.[4,46,60,64]

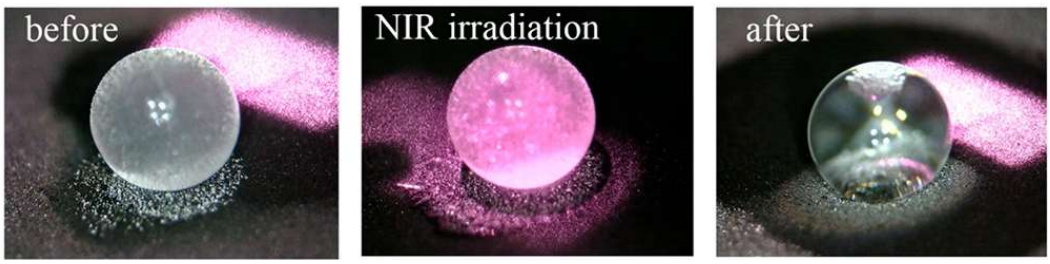

Fig. 5. Ice droplet melting under NIR irradiation. Reproduced with permission from ref.[42] Copyright 2018 American Chemical Society.

Apart from measuring the water melting in the form of droplets, some experiments were conducted on spilled water,[88,94] ice cubes[33,40,53,78] or a bottle with frozen water inside.[72]

The deicing time was also defined as the time needed for the water droplet to melt and depart from the angled surface. For that purpose, it is placed in a climate chamber in a tilted way (**Fig. 6**), and time is measured from the turning on of the power (solar, electric, *etc.*) to the droplet skidding.[35,51,52,68]

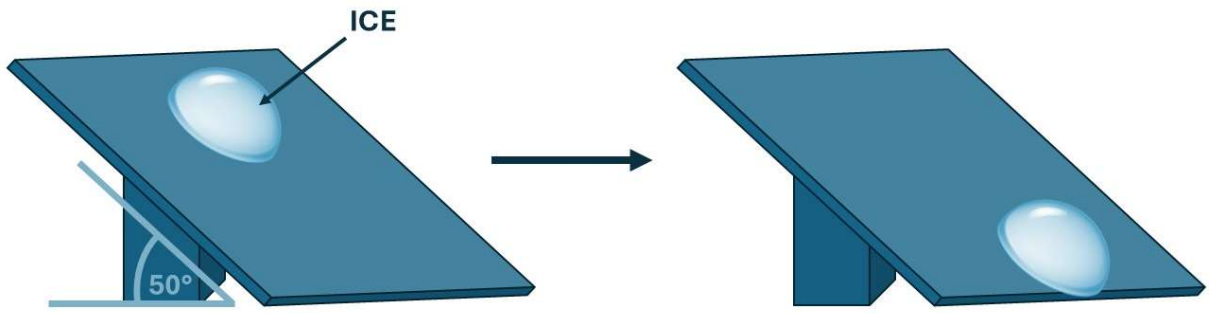

Fig. 6. Droplet melting and departure from slippery slope. Adapted from ref.[52] Copyright 2020 Elsevier.

For natural condition simulation, apart from examining pure, distilled water, Liu *et al.* experimented with opaque, muddy water droplets melting and sliding down the slope under photoelectrothermal circumstances. To obtain a full revision, they examined outdoor snow removal on sunny and cloudy days and at night.[60]

3.3. Ice accumulation

Mokarian *et al.* first measured the weight of accumulated ice. The coated and uncoated aluminum plates were weighed and placed at a 45° angle in the lab refrigerator set at –20° C and 90% relative humidity for 45 min, and then the weight of accumulated ice was measured and compared.[37] Zhang *et al.* presented a self-made chamber for water dripping test for anti-icing effectiveness measurements (**Fig. 7**). The chamber was set at –10° C, and the ice-water mixture was dripping from the funnel onto the surfaces placed at a tilted angle of 30° for 30 min. After that, the surfaces were photographed, and the amount of accumulated ice was compared.[41] Rajiv *et al.* used supercooled water (–20° C) instead of a climate chamber and compared photographs.[43] A similar approach was presented by Eseev *et al.* in which samples were placed on an angled Peltier element, and the droplets were applied from a microburette.

The droplets rolled off the sample to the cuvette, where they were weighed, and the collected mass was compared for the coated and uncoated samples.[87]

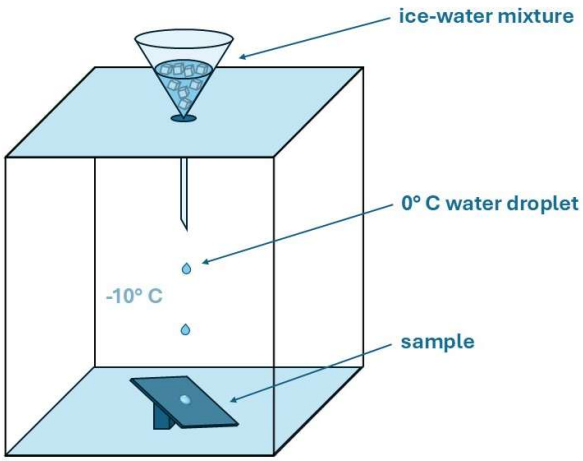

Fig. 7. Chamber for water dripping test. Adapted from ref.[41] Copyright 2018 Elsevier.

3.4. Frosting/defrosting time

To indicate frosting time, specimens are placed in a humid environment (90% RH) and attached to a cooling table. The process is complete when the sample is fully covered with frost.[32,53,70] Wei *et al.* additionally characterized the growth of frost thickness.[96] In turn, defrosting time was presented as a period needed for complete melting of an ice cover with a defined thickness, with a power supplied by, *e.g.*, DC input,[54] NIR lamp,[63] a sunlight lamp,[44,53] or a microwave oven.[77,78] Additionally, Wang *et al.* proposed the glaze ice test, in which they placed a commercial moisturizer in a climate chamber.[54] The examined plates were set at a tilting angle of 30°. After creating a 3-mm ice cover, they applied a DC voltage or an NIR lamp. For this type of experiment, the time to ice detachment from the surface is measured, and it is observed if the water droplets stay on it.[39,45,54,68,85]

Liu *et al.* examined surfaces attached to a thermal-conductive plate cooled by a cryogenic circulator, enabling the formation of a 2-mm ice cover. They also considered a situation in

which sunlight reaches the coating partially, like in nature, and experimented with irradiation on only half of the surface and observing whether the frost disappeared from the whole area. Finally, they conducted an outdoor test for snow melting on a sunny winter day.[59]

Defrosting time was also measured on curved surfaces,[75] or even real rotor blades (**Fig. 8**).[29,48,86,93] Fisher *et al.* placed the blade sprinkled with water in the climate chamber set to –10° – 0° C and exposed it to an air stream of 7 m s^{-1}. The ice cover was 3–4-mm-thick, and they measured the time to complete deicing under a set voltage.[93]

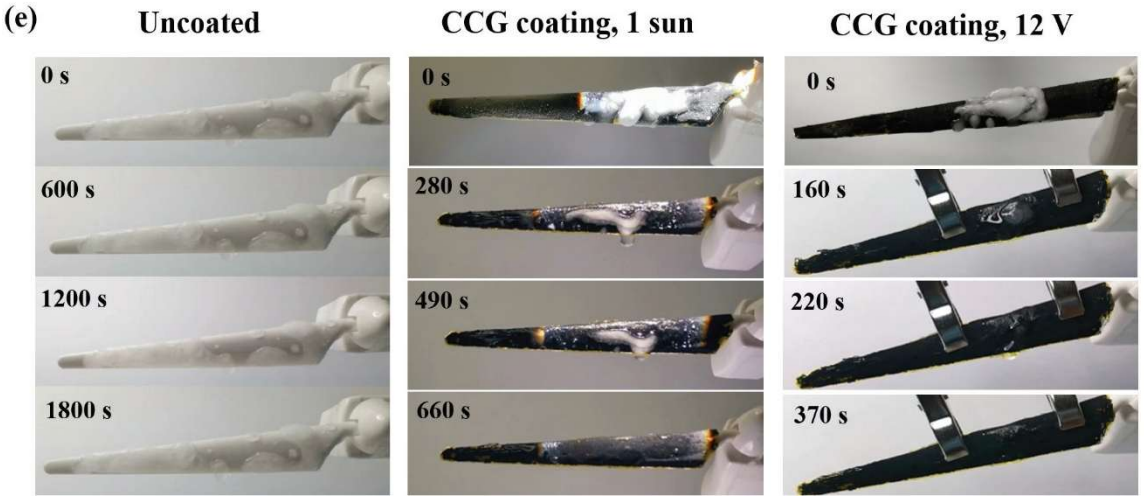

Fig. 8. Deicing process on a real rotor blade. Reproduced with permission from ref.[86] Copyright 2023 Springer.

3.5. Flow environment

Zhao *et al.* prepared a custom-made climate chamber, as shown in **Fig. 9**, for examination in a flow environment. The plastic square tube enabled a defined flow of cold wind. The sample was placed at an inclination angle of 30–45°, and the ice accumulation area was examined and compared.[51,52]

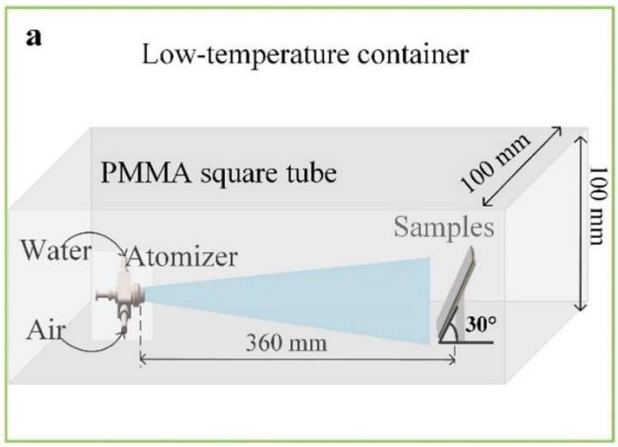

Fig. 9. Custom-made climate chamber for flow environment experiments. Reproduced with permission from ref.[52] Copyright 2020 Elsevier.

4. Photothermal coatings

Ultra-black CNTs as light absorbers have the potential to create warm surfaces with anti-icing and deicing properties. On that basis, Lin *et al.* constructed a coating composed of CNTs mixed with water-based polyacrylic resin and vinyl chloride resin. The dispersion was sprayed on an aluminum plate and laser etched to remove the pure resin film from the top of the surface. As a result, 60-s xenon lamp irradiation of the coating enabled temperature increase from 30.8 to 104.6° C. Under 1 sun illumination at –20° C, the frosting time was 12.3 times longer than that of an aluminum plate.[32] Another photothermal approach used SiO_2 aerogel mixed with carboxylated MWCNTs, applied on the insulated glass slide. The photothermal performance was measured under near-infrared light irradiation with a power of 1 W. They demonstrated that the amount of CNTs in the coating positively correlates with the photothermal heating rate. For the coating with the highest CNT content (0.8%), the temperature increased from 5° C to 158° C over 626 s. The deicing capability was presented by complete melting of the 3-mm-thick ice cover for just 230 s.[89]

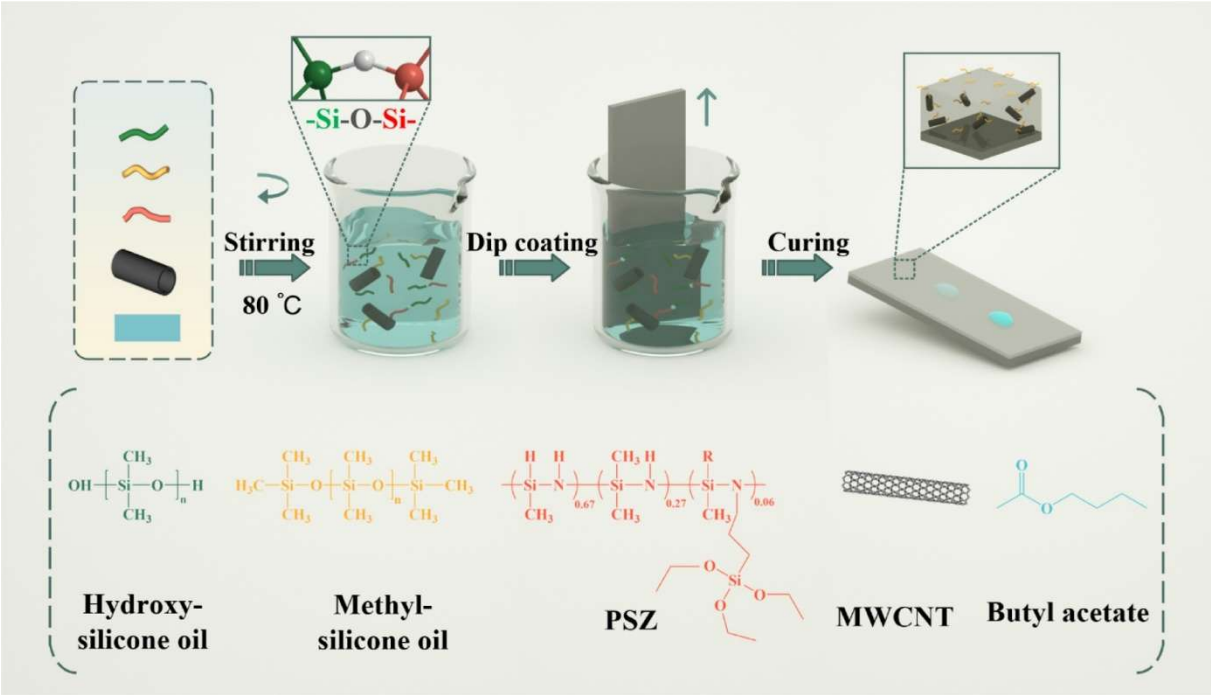

Fig. 10. Preparation of SLIPS photothermal coating. Reproduced with permission from ref.[91] Copyright 2024 Elsevier.

Prevalent improvement of anti-icing/deicing properties is inspired by the Nepenthes pitcher plant, slippery liquid-infused porous surface (SLIPS). The approach is appropriate for CNT coating due to its porous morphology and low surface energy. Among photothermal coatings, several lubricating liquids are applied, *e.g.*, paraffin,[39,40,71] silicone,[53,71,91] and coconut oils.[75] The coating composed by Ma *et al.* (**Fig. 10**) was applied by dip coating of aluminum plate in dispersion of MWCNTs, hydroxy-terminated and methyl-terminated silicone oils, and polysilazane (PSZ). The photothermal performance of the coating was exhibited by the temperature increase from –10° C to 140° C in 5 s under 2.5 W cm^{-2} irradiation intensity. The droplet froze 4 times slower than on the aluminum surface, and under 2.5 W cm^{-2} irradiation, it melted in 21 s.[91]

5. Electrothermal coatings

Electrothermal coatings, as an active means of ice protection, use Joule / resistive heating, which is highly efficient and easy to fabricate. Some published attempts applied ready-to-use MWCNT dispersions for scalable roll-to-roll printing of films.[88,93] Fischer *et al.* coated the textile with the use of rotary-screen printing, resulting in a sheet resistance of 26 kΩ sq^{-1},[93] while Rashid *et al.* used the slot-die coating method on PET foil, giving films with a sheet resistance of 6.53 kΩ sq^{-1} and melting a 12-g ice block in 3 min at an applied voltage of 40 V DC.[88] Another approach, using a commercial solution, applied a ready-to-use paste of poly(3,4-ethylenedioxythiophene)-coated SWCNT sprayed on top of a multilayer MXene composite for wind turbine blades. The composite enabled ice detachment from vertically positioned samples within 5 min at a heating power density of 0.088 W cm^{-2}.[31]

Suited to aviation requirements, MWCNT dispersions in distilled water using sodium dodecylbenzene sulfonate were proposed.[4,5] Hong *et al.*'s idea employed the spin-coating method, resulting in the water droplet melting in 56 s under 50 V.[4] Jung *et al.* used the spray-coating method, and the water droplet melted after 350 s with an applied voltage of 40 V.[5]

PU as a matrix was found helpful as a binder in several approaches.[31,51,52] Zhao *et al.* developed a sandwich-like coating with a MWCNT-PU layer between two silver electrodes, enabling the deicing and detachment of the droplet from the slippery slope after 49 s at a heating power density of 0.5 W/ cm^{-2}.[52] As an improvement, the same research group developed a MWCNT coating consisting of a mixture of PU and paraffin applied as a one-layer coating, facilitating faster water droplet departure (45 s) at a lower heating power density (0.3 W cm^{-2}).[51] Zhou *et al.* presented a three-layer CNT concentration gradient coating with water-soluble PU (WPU) as a matrix (**Fig. 11**). This specific construction hindered heat dissipation downwards and promotes heat transfer to the upper layers. As a result, the coating prevented ice formation for

60 s at –15° C under 30 m s^{-1} flow conditions and 8.5-mm-thick ice melted in 22 s at a power density of 1.8 W cm^{-2}.[31]

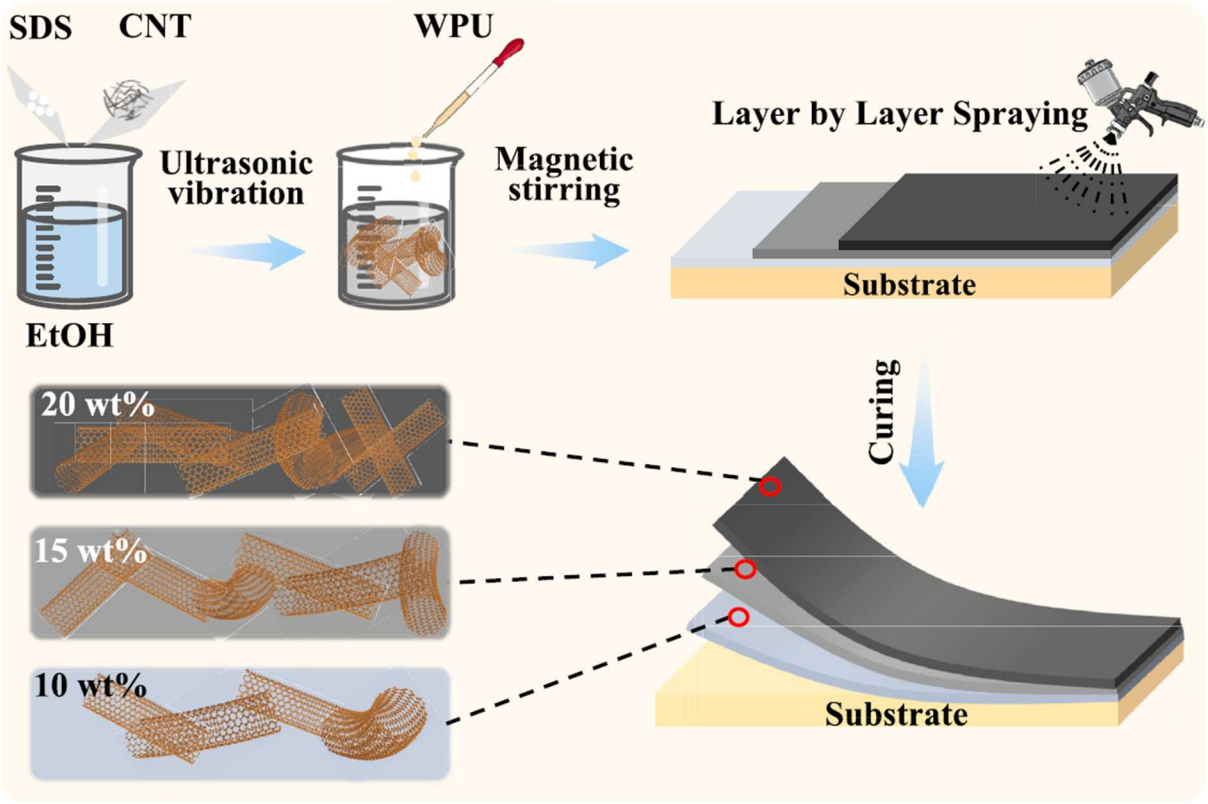

Fig. 11. Preparation of three-layer CNT concentration gradient coating. Reproduced with permission from ref.[31] Copyright 2025 Elsevier.

6. (Super)hydrophobic coatings

Biomimicry-inspired superhydrophobic surfaces are promising next-generation ice-proof materials. Functionalization or adding polymers and fillers improves the water repellency of CNT-based coatings. Mokarian *et al.* presented the first application of CNTs in anti-icing superhydrophobic coatings. The pristine MWCNTs and silicone rubber dispersion were applied to a glass slide using a dropper, resulting in a WCA of 159.3°. The anti-icing test showed that the weight of accumulated ice on the coating was 55% lower than on the glass plate.[37] Similarly

to this approach, other researchers constructed icephobic coatings with various binders – epoxy resin,[41] acrylic acid,[76] PDMS,[69] vulcanized silicone rubber,[61] and PVDF with poly(vinyl acetate).[81]

Additional nanofillers facilitate the creation of hierarchical micro-nanostructures similar to the lotus leaf. Published attempts applied particles such as zinc oxide,[38] silicon carbide,[62] or CNFs.[43] Rajiv *et al.* composed a CNT-CNF coating using the supercritical fluid processing method to improve its effectiveness at low temperatures. Owing to this treatment, the coating WCA increased from 160° to 171.6°, resulting in no ice adhesion in the supercooled water dripping test.[43]

Functionalization aims to increase the roughness and decrease the surface energy of CNT. In superhydrophobic coatings, CNTs are modified with polystyrene,[50] and through functionalization with silicon dioxide particles[56,81] covered with perfluorocarbon chains[62,81] or long-chain hydrocarbons.[56] Zhang *et al.* applied SiO_2 nanoparticles reacted with the carboxylated MWCNTs using 3-aminopropyltriethoxysilane to create a MWCNT-SiO_2 hybrid. The obtained composite was modified with 1*H*,1*H*,2*H*,2*H*-heptadecafluorodecyl-trimethoxysilane and mixed with poly(vinylidene fluoride) (PVDF) and poly(vinyl acetate) (**Fig. 12**) to obtain WCA equal to 163.5° and delayed freezing time for 5 min at –20° C. The presented approach was dedicated to marine equipment and additionally characterized by effective anti-corrosion and drag reduction properties.[81] Both silicon carbide and functionalization of the nanofiller surfaces were attempted by Xue *et al.* Similarly to the previous approach, CNTs were mixed with SiO_2 precursor, perfluorooctyltriethoxysilane, and dual-size SiC. Epoxy resin and vulcanized silicone rubber were used as film-forming polymers. The obtained dispersion was sprayed onto an aluminum board, resulting in a WCA of 167.4° and a freezing time 3.77 times lower than that of the bare surface. Composed coating also

exhibited great mechanical, chemical, and high-temperature resistance, self-cleaning, and anti-corrosion properties.[62]

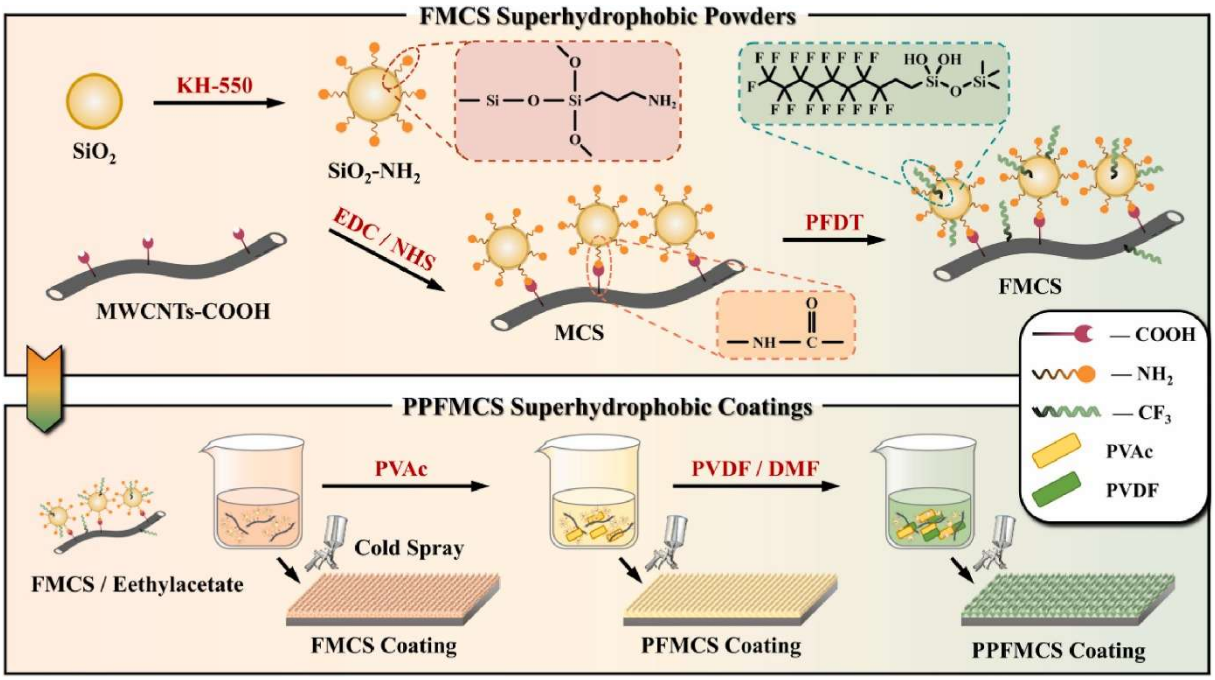

Fig. 12. Preparation of superhydrophobic coating based on MWCNTs-SiO_2. Reproduced with permission from ref.[81] Copyright 2024 Elsevier.

Among superhydrophobic anti-icing surfaces, Essev *et al.* presented a unique perspective. They created a MWCNT xerogel and sprinkled it on steel plates with adhesive. Two sprinkled steel samples were pressed together and milled until uniformity in the MWCNT coating. Finally, the surface was lubricated with perfluorodecalin as an example of following the SLIPS approach. The coating exhibited a water contact angle of 155.6°, and the rate of ice formation in the water dripping test was several times lower compared to pure steel.[87]

7. Synergistic strategies

Photo-electrothermal coatings. Although photothermal deicing is inexhaustible and clean, it is limited under low-light conditions, which electrothermal materials can complement.

Conversely, supplementing electrothermal deicing with photothermal assistance reduces energy consumption. The construction of layered coatings enables an effective combination of these two strategies, with surface lubrication as an additional improvement. Xiao *et al.* used a dispersion of MWCNTs, graphite powder, and PDMS in the electrothermal layer,[71] while Chai *et al.* applied CNTs dispersed in a PU matrix in the photothermal layer.[75] In the first attempt, the synergistic action of the photo and electrothermal layers enabled 3 times longer ice prevention compared to the single-strategy approach.[71] In the second research, the photoelectrothermal coating rapidly melted the frost layer within 60 s, and 10-μL water droplets remained unfrozen until completely evaporated.[75]

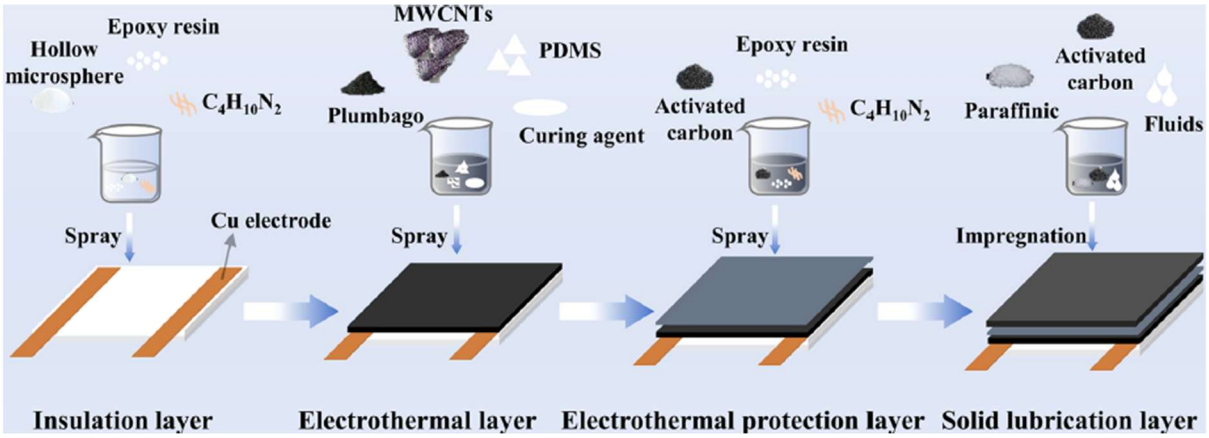

Fig. 13. Preparation of photo-electrothermal coating with lubrication layer. Reproduced with permission from ref.[71] Copyright 2024 American Chemical Society.

7.1. Superhydrophobic and microwave-heated coatings

Enriching active microwave-heating deicing with passive superhydrophobic anti-icing is not only a complementary approach but also enables prevention from both water penetration and secondary ice formation, which is crucial for roads and pavements. CNTs are suitable for both microwave absorption and building a superhydrophobic surface. They were sprinkled on uncured acrylic road paint applied to an asphalt sample, demonstrating a WCA of 161.2° and 1.63-times prolonged time of droplet freezing.[77] As its microwave energy utilization efficiency

is only 42%, Jia *et al.* proposed an improvement in coating construction with a micro-sized iron powder layer (**Fig. 14**). Consequently, they achieved an energy utilization efficiency of 47% with a microwave melting rate of 8.37 g min^{-1}.[78]

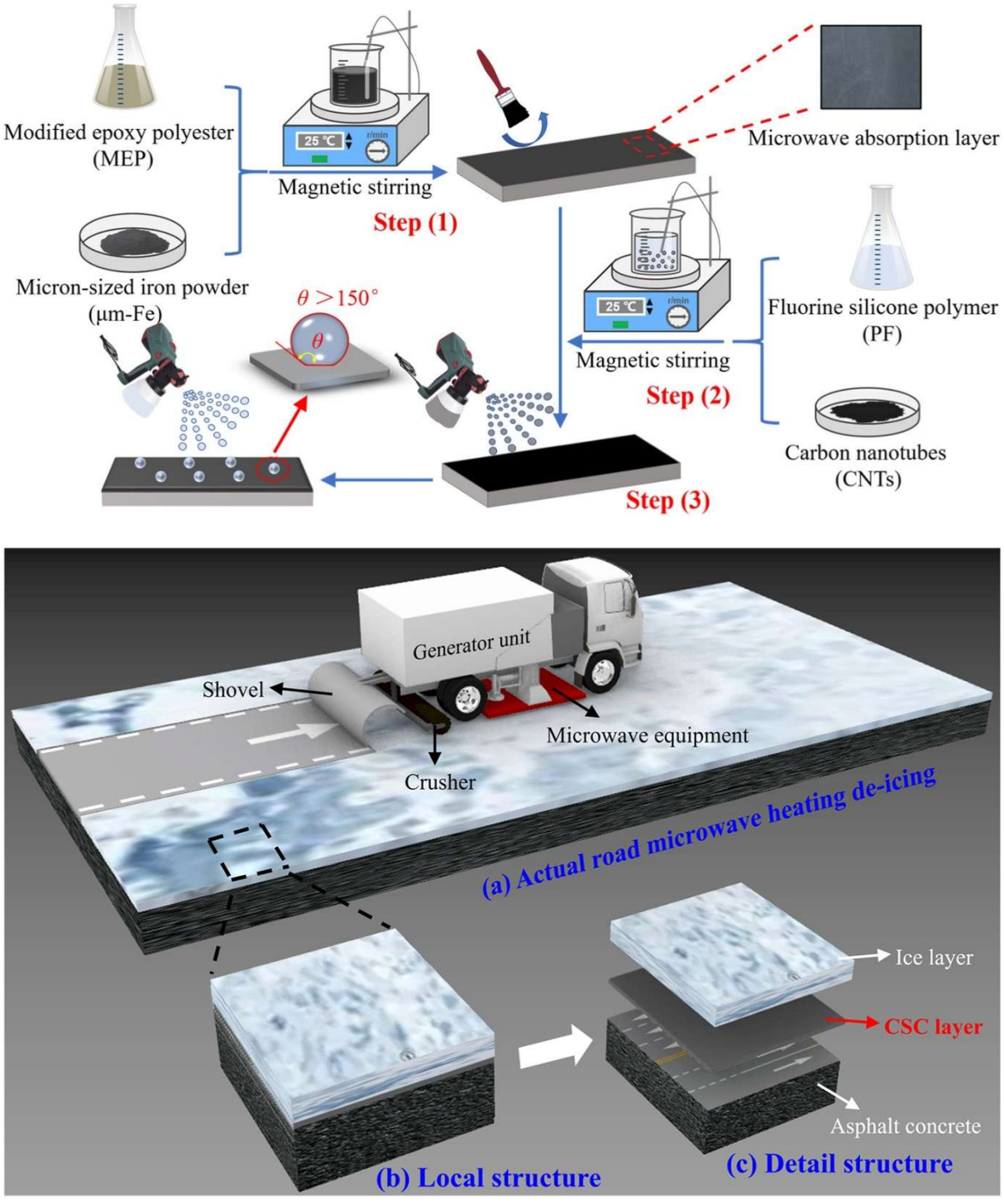

Fig. 14. Preparation process of microwave-heated and superhydrophobic coating for roads and pavements. Reproduced with permission from ref.[78] Copyright 2024 Elsevier.

7.2. Superhydrophobic electrothermal coatings

A hybrid superhydrophobic and electrothermal coating can be constructed in a single combined layer using modified MWCNTs or in two individual layers with pristine MWCNTs. A primary attempt involved applying a single layer composed of a hierarchical structure of graphene, fluorinated CNTs, and silica nanoparticles obtained by evaporation of dispersants including THF and ethanol. The prepared surface demonstrated a freezing time almost 6 times longer than the bare substrate, with rapid deicing (70 s) at a voltage of 50 V.[85] Fluorinated MWCNTs were also found to be helpful in a low-pulse voltage approach. When mixed with epoxy resin, the resulting coating exhibited a delay in freezing time of up to 8 h at 15 V with a frequency of 10 s/100 s.[34]

Fan *et al.* proposed a multilayered approach in which a CNT heat-transfer coating was applied on both sides of a silver-copper electric-heating coating and covered with a superhydrophobic layer made of epoxy resin, silica nanoparticles, kaolin clay, and hexadecyltrimethoxysilane. The obtained surface resulted in a 6.5-times longer droplet freezing time than an uncovered glass slide, and a deicing time of 78 s, with an electrical power consumption of 0.2 W.[64] A unique attempt was presented by Suryaprabha *et al.*, in which the coated substrate was cotton fabric. The multilayer coating consisted of a MWCNT layer, a ferrite layer, a nickel nanochains layer, and a PDMS superhydrophobic layer. Apart from its ice-phobic properties, the coating also provided electromagnetic interference (EMI) shielding, motion monitoring, and an underwater SOS (**Fig. 15**). Regarding deicing potential, under an applied voltage of 6 V, the bottle full of ice placed on the superhydrophobic fabric completely melted within 40 s, which was 30 times faster than on conventional cotton fabric.[72]

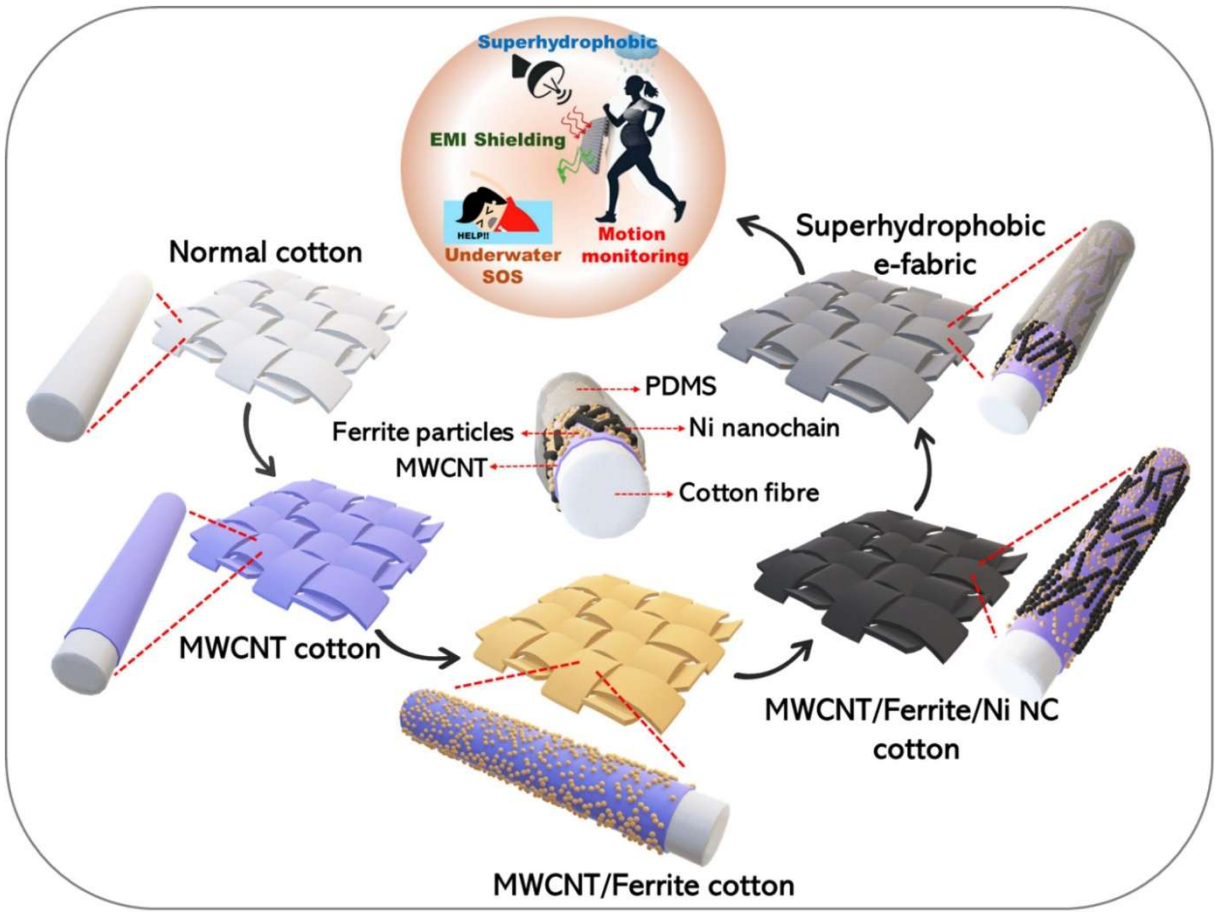

Fig. 15. Multilayer superhydrophobic electrothermal coating for fabrics. Reproduced with permission from ref.[72] Copyright 2025 Elsevier.

7.3 Superhydrophobic photothermal coatings

There are hybrid approaches that utilize pristine MWCNTs only as light absorbers in superhydrophobic photothermal coatings. The superhydrophobicity of the coating can be achieved by adding a top layer. Jiang *et al.* proposed a two-layered coating composed of PVDF and MWCNTs covered with 1*H*,1*H*,2*H*,2*H*-perfluorodecyl-trimethoxysilane. They obtained a WCA of 163°, and the freezing time of the droplet was 584 s.[44] Dedicated for covering concrete, Gu *et al.* developed a MWCNT-PDMS coating with a top layer of a superhydrophobic commercial coating. The results showed WCA was 162°, the freezing time was delayed almost

4.5 times compared to bare concrete, and the coating could completely melt ice in 0.56-times the melting time on concrete.[67]

In some approaches, the dispersion of pristine CNTs and polymeric binder was sufficient to ensure both the photothermal effect and superhydrophobic properties. Binders applied for that purpose were PTFE,[80] fluorineoligomer-modified epoxy resin,[82] and epoxidized soybean oil. The last-mentioned, in addition to its ice-phobic properties, as a biobased solution, offered closed-loop recyclability.[83]

Similar to superhydrophobic coatings, additional powders were applied to polymeric binders to enhance their hydrophobic properties without the need for functionalizing CNT. Deng *et al.* synthesized mesoporous silica nanoparticles loaded with PDMS and mixed them with CNTs and silicone resin, resulting in a coating exhibiting nearly 73 times longer freezing time than on a bare aluminum plate.[29] Peng *et al.* combined anti-freeze protein-modified emulsified asphalt with silicone caribe/CNT-based coating, obtaining protection suitable for pavements and roads. The prepared surface was characterized by a 160.4° WCA and 11 times longer freezing time under 1 kW m^{-2} than on the conventional asphalt.[84]

Sun *et al.* developed a coating composed of MWCNTs and octadecyltrichlorosilane (OTS) obtained by magnetic stirring and spraying onto a copper sheet. They achieved a WCA of 158.3°, 150 times longer freezing time than on the pure copper sheet, and a 50–60% decrease of initial melting time under light compared to bare substrate.[92] Wei *et al.* presented an improvement to this method, adding ultrasonication to the preparation process, which increased the WCA to 163°. They assessed ice-phobic properties, indicating a 373%-longer frosting time than on Cu.[96] Zhang *et al.* enriched the formula with carbon black and PDMS for concrete impregnation, resulting in a 3.22-times longer freezing time than on the bare surface. Under simulated sunlight irradiation (100 mW cm^{-2}), the coating melted the frozen droplets within 176 s.[73] Additionally, for a concrete application, Li *et al.* used carboxylated MWCNTs instead

of pristine ones to enhance the surface coverage with OTS. They additionally adsorbed *n*-tetradecane on the CNT surface to impart phase-change functionality. The dispersion of modified CNTs was sprayed onto concrete specimens covered with epoxy resin as a primer. As a result, it extended the droplet freezing time by a factor of 10.[95] As an alternative to carboxylation, modification with dopamine hydrochloride was also introduced.[66] Another long-chained hydrocarbon, *n*-dodecylamine, was connected to the surface of the CNT through pretreatment with dopamine hydrochloride (**Fig. 16**). As-prepared modified MWCNTs were dispersed in silicone resin, resulting in a coating with a WCA of 162.5°. A 2-mm-thick ice cover was melted entirely after 423 s of 1 sun irradiation.[45]

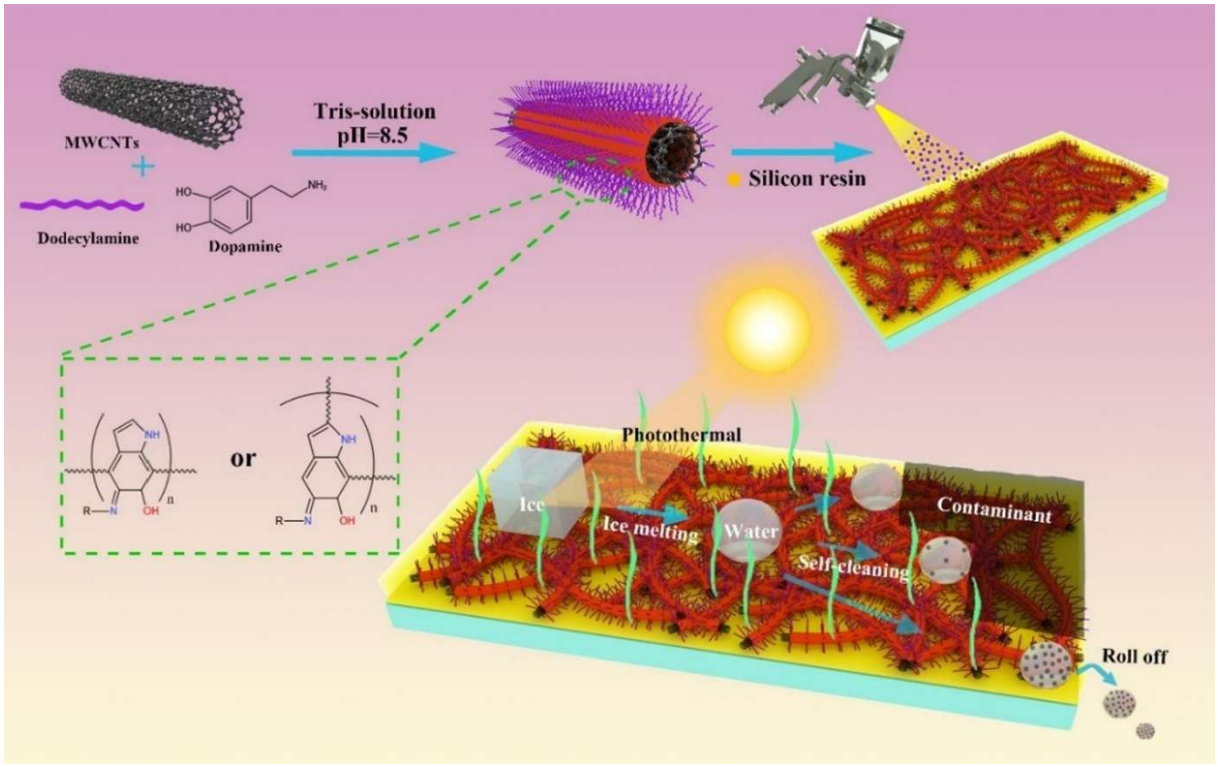

Fig. 16. Preparation of superhydrophobic photothermal coating with *n*-dodecylamine modified MWCNTs. Reproduced with permission from ref.[45] Copyright 2022 Elsevier.

Composites with silica nanoparticles were introduced to improve the dispersibility of CNTs. Zhang *et al.* proved that the most effective weight ratio of CNT/SiO_2 for coating in epoxy resin was 1:3[63] and Guo established a similar ratio for PDMS-based coating – 1:2.5.[48] Epoxy resin-

based coatings were found useful for cement impregnation. By adding a layer of modified CNTs treated with perfluorodecyltrichlorosilane, Li *et al.* obtained a coating with a WCA of 159.6° and a 16-times longer freezing time.[30] As an alternative for the cement industry, SiO_2-CNT was covered with dodecyltrimethoxysilane and additionally impregnated with *n*-tetradecane.[65]

A significant group of photothermal superhydrophobic coatings utilizes fluorinated MWCNTs. Applied fluorinating agents included perfluoroalkyl chains of different lengths and linking groups (siloxane or silane)[42,46,59] or polymer, especially poly(methyl-3,3,3-trifluoropropyl siloxane) (PMTFPS).[55,79] Perfluoroalkyl chains were introduced directly on the CNT surface,[42,46] or through pre-coverage with polydopamine.[59] Applied individually, they resulted in a lower WCA than when combined with other microstructures. Jiang *et al.* developed a coating based on fluorinated MWCNTs and SiC (mass ratio of 1:2), which enabled the complete meltdown of 3 mm-thick ice cover within 250 s under near-infrared irradiation.[42] Zan *et al.* created a papilla-like microstructure by adding polydopamine-coated layered basic zinc acetate microparticles to cover wood, PTFE, fiber-reinforced plastic, aluminum alloy, and glass. It could effectively prevent ice formation for 112.5 min at −10° C and 75 ± 5% relative humidity.[46] Liu *et al.* proposed decorating coatings with PMTFPS using only MWCNTs[55] and in a mixture with fluorinated SiO_2.[79] They obtained 11.6 times longer freezing time for only-CNT coating,[55] and 15.25 times for the mixture.[79]

Other CNT surface modifications concern coating with silver,[33] titanium oxide,[47] biochar nanoparticles,[49] and metal-organic framework (MOF) nanoparticles.[74] Reaching for simpler preparation, Liu *et al.* presented a TiO_2-decorated MWCNT-based coating that exhibited a freezing time 12 times longer and a deicing time 11 times shorter.[47] Following sustainable trends, Liu *et al.* applied polydopamine-modified CNTs to functionalize their surface with silver and developed an all-waterborne process, but still using a fluorine-containing binder.[33] Lei *et al.*, aiming for both simpler and greener processes, successfully eliminated fluorine by applying

rice-originating biochar, nevertheless, with the use of organic solvents.[49] Zhang *et al.* proposed growing a nano-MOF on the CNT and increasing their hydrophobic properties with octanoic acid. It resulted in the complete evaporation of supercooled droplets before their condensation at –40° C and approximately 30% relative humidity.[74]

7.4. Superhydrophobic photoelectrothermal coatings

Superhydrophobic photoelectrothermal coatings are the most complex approaches; however, they offer solid prevention independent of weather conditions, time of day, and continuity of power supply (**Fig. 17**).

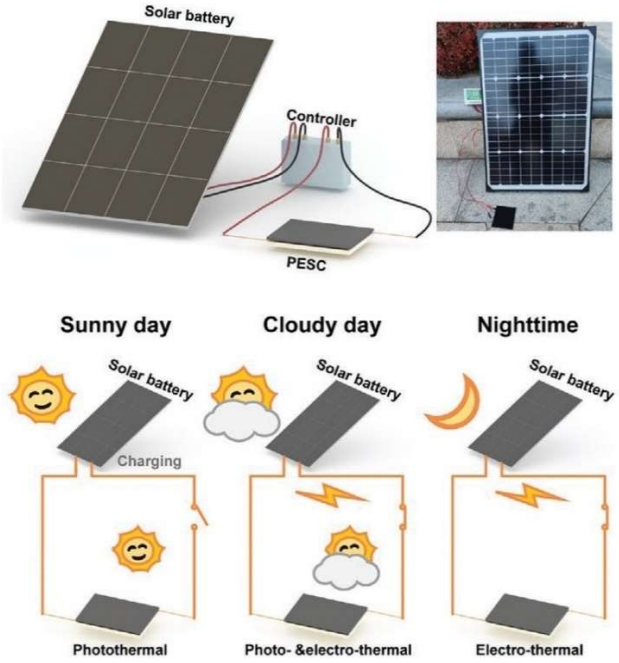

Fig. 17 All-day ice prevention of superhydrophobic photoelectrothermal coating. Reproduced with permission from ref.[60] Copyright 2021 Wiley.

Coatings based only on pristine CNTs as a nanofiller, enabling light absorption, electroconductivity, and superhydrophobicity, were developed with the use of binders: fluorine-modified polyacrylate,[60] PDMS,[70] and thermoplastic elastomer.[90] Peng *et al.* presented a three-

layer coating in which the aluminum substrate was first covered with PDMS, the middle layer was composed of MWCNTs and PDMS, and polypyrrole/PDMS was sprayed on top. The produced coating exhibited a 14-times longer freezing time of droplets; under 1 sun simulated solar irradiation, a 60-s defrost time, and a 360-s deicing period; at an electric power density input of 0.20 W cm^{-2}, a 120-s defrost time.[70]

The multi-purpose properties of pristine CNT in superhydrophobic photoelectrothermal coatings may be improved by mixing with other powders. Chang *et al.* used fluorinated silica to endow a hierarchical porous structure. The dispersion without any binder was sprayed onto the poly(amide-imide) thermal insulating surface, which resulted in 4 times longer freezing, 500 s of electro-deicing at 36 V, and 120 s of photo-deicing under light irradiation with a power of 0.2 W cm^{-2}.[35] Cheng *et al.* proposed a coating composition consisting of MWCNTs, rGO, and hydrophobic surfactant cellulose 1-butylimidazolium bis(trifluoromethane)sulfonimide originating from natural cellulose. They covered the blade of a wind power generator and observed complete deicing after 660 s under 1 sun condition and after 370 s at 12 V.[86] Fluorine-containing binder (PVDF), accompanied by PDMS, was also applied by Jiang *et al.* in a coating composed of MWCNTs, graphite powder, and titanium nitride. They achieved 14 times longer freezing time. With photothermal heating of 0.05 W cm^{-2} and 0.027 W cm^{-2} electrothermal heating, the ice bead completely melted after approximately 323 s.[57] Huang *et al.* constructed a sandwich-structured coating, in which a middle layer consisted of CNTs, graphene closed between two layers of PDMS, and finally sprayed with a dispersion of silica, titanium nitride, and PDMS. As a result, the coating prevented droplet freezing for 213 s without any power supply and under 1.8V and 0.8 sun, the droplet remained unfrozen for up to 2400 s.[68]

In Guo *et al.*'s work, fluorine-free improvement of superhydrophobic properties was ensured by surface modification of MWCNTs with cetyltrimethylsiloxane. The coating exhibited a 25.7-times longer freezing time at –10° C and achieved photothermal (1.5 sun) defrosting in 237 s

and electrothermal defrosting at 25 V in 35 s.[36] Wang *et al.* modified MWCNTs with perfluorooctyltriethoxysilane and constructed a hierarchical micro-nano structure with carbon powder. The coating was applied to poly(urea–urethane), and the ice could be completely melted within 120 s when the synergistic anti-icing strategy was utilized.[54] Mei *et al.* proposed a multi-layer coating using MWCNTs functionalized with iron(III) oxide. Silver-plated aramid paper was scraped with modified CNT-PDMS dispersion and then covered with carbon black, graphite powder, and PDMS topcoat. The coating completely melted a water droplet in 210 s at 0.1 W cm^{-2} electrical power and in 180 s at 1 sun.[58]

8. Hansen Solubility Parameters

The anti-icing efficacy of CNT-based coatings is intrinsically linked to their physicochemical surface characteristics, particularly surface energy and interfacial interactions, both of which can be quantitatively described using Hansen Solubility Parameters (HSPs). The HSP framework divides the total cohesive energy density of a material into three components: dispersion forces (δ_d), polar interactions (δ_p), and hydrogen bonding (δ_h).

In the context of ice-phobic materials, particularly those containing CNTs, the relevance of HSPs arises through two primary mechanisms: (i) control of surface energy and wettability, which governs water repellency and ice adhesion strength, and (ii) interfacial compatibility within nanocomposite matrices, which determines the uniformity of CNT dispersion, hierarchical surface morphology, and, ultimately, the functionality of the coating (Fig. 18).

Hydrophobicity and ice adhesion reduction are strongly correlated with materials exhibiting low δ_p and δ_h values, indicative of low polar and hydrogen bonding capacity, respectively. For instance, pristine MWCNTs possess moderately hydrophobic character, with $\delta_{total} \approx 18–20$ $MPa^{1/2}$, but their performance can be significantly enhanced through surface fluorination.[34,44,84] The introduction of perfluorinated moieties, *e.g.*, perfluorodecyltrimethoxysilane, onto the CNT

surface reduces both δ_p and δ_h toward values characteristic of low-surface-energy materials like PTFE, resulting in WCA exceeding 160° and dramatic reductions in hydrophilicity and ice adhesion strength, often below 40 kPa.[44] This enhancement is rooted in classical heterogeneous nucleation theory, which relates the free energy barrier (ΔG^*) for ice formation to both the interfacial energy between solid and liquid phases and the WCA. High WCA values (>150°), typically achieved via HSP-guided surface modifications, increase ΔG^*, thereby delaying nucleation and reducing the probability of ice formation.[92]

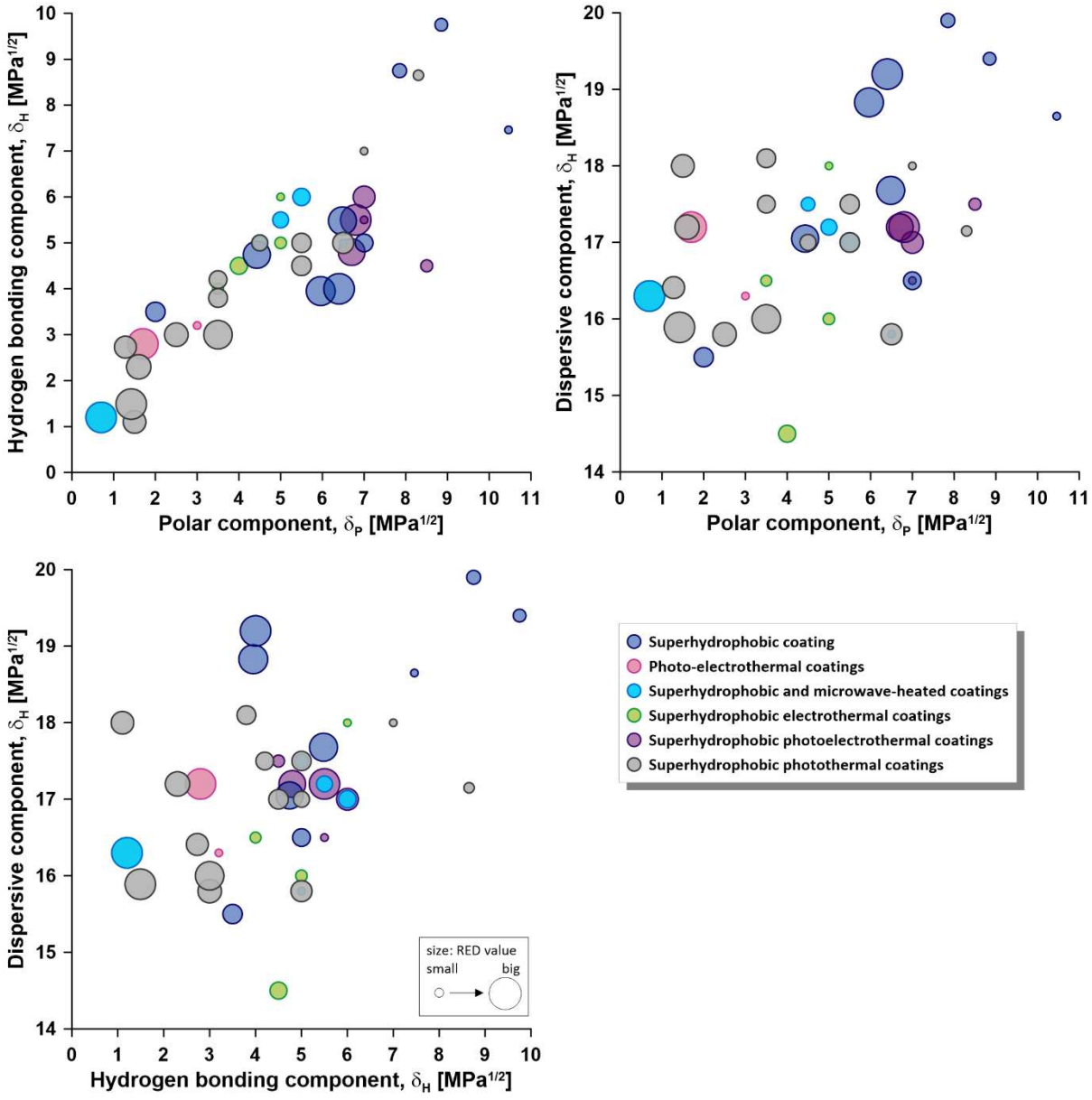

Fig. 18. Relation between the HSP component and ice resistance expressed by RED parameter.

Moreover, HSPs play a critical role in governing the dispersion stability of CNTs in polymeric matrices.[5,29,31] Incompatibility between the HSPs of CNTs and the host matrix leads to aggregation, resulting in surface heterogeneity and compromised anti-icing behavior due to poor nanostructure formation. Functionalization strategies, such as oxidation (introducing carboxyl, hydroxyl, and other groups), silanization, or fluorination, allow for modulation of the CNT surface HSPs to better match the solubility parameters of the matrix polymer (*e.g.*, PDMS, epoxy resin, PU). For example, PDMS exhibits $\delta_{total} \approx 15.5–16.5$ MPa$^{1/2}$, and appropriate functionalization of CNTs to achieve a similar HSP value ensures optimal dispersion, uniform micro-/nanostructuring, and effective thermal or electrothermal pathways essential for rapid de-icing applications.

De-icing time is typically governed by the efficiency with which thermal energy is delivered to the ice/coating interface and the *rate at which water can detach or drain* from the surface after melting. HSPs influence this process in two primary ways:

– *thermal contact resistance* and *phase boundary stability* – the HSP mismatch between water ($\delta_{total} \approx 47.8$ MPa$^{1/2}$) and the coating surface contributes to thermal boundary resistance (Kapitza resistance), where hydrophobic (low δ_p and δ_h) surfaces reduce energy transfer between solid and liquid phases, thereby localizing heat at the interface, accelerating melting; for CNT-based photothermal or electrothermal coatings, low δ_p and δ_h values correlate with higher WCA and less interfacial wetting, allowing the molten layer to detach more easily, thus *reducing de-icing time*,

– *water mobility and drainage* – superhydrophobic surfaces derived from low HSP values exhibit Cassie–Baxter wetting states, where water contacts only the top of surface asperities. This reduces contact area and adhesion, allowing melted water to *slide or roll off quickly*, a key factor in rapid de-icing.

Guo *et al.* demonstrated that coatings incorporating fluorinated silica-grafted CNTs ($\delta_p \approx 1$ $MPa^{1/2}$) were able to melt a 2-mm-thick layer of ice in just 175 s under 1.5 sun irradiation and in 35 s with a 25-V electrothermal input.[36] This performance surpassed that of coatings with carboxylated CNTs, which, despite having higher δ_p and δ_h values, retained more water due to stronger hydrogen bonding.

In lubricated surfaces, such as those based on SLIPS, the HSP compatibility between the CNT-structured porous matrix and the infused lubricant (*e.g.*, silicone oils or fluorinated liquids) is vital for long-term functionality.[91] A suitable match ensures capillary retention and prevents lubricant drainage during environmental cycling. If the $\Delta\delta$ (difference in solubility parameters) between the matrix and lubricant exceeds ~5 $MPa^{1/2}$, dewetting and phase separation may occur, reducing the material anti-icing capacity over repeated freeze–thaw cycles. Furthermore, HSPs can be leveraged to predict and tailor synergistic effects in multifunctional coatings, such as those combining photothermal, electrothermal, and superhydrophobic strategies. For example, CNTs functionalized with both fluorinated chains and conductive dopants can simultaneously optimize δ_p and δ_h for enhanced water repellency, while preserving the thermal conductivity and electrical pathways required for active de-icing under solar or electrical stimulation (**Fig. 18–20**).

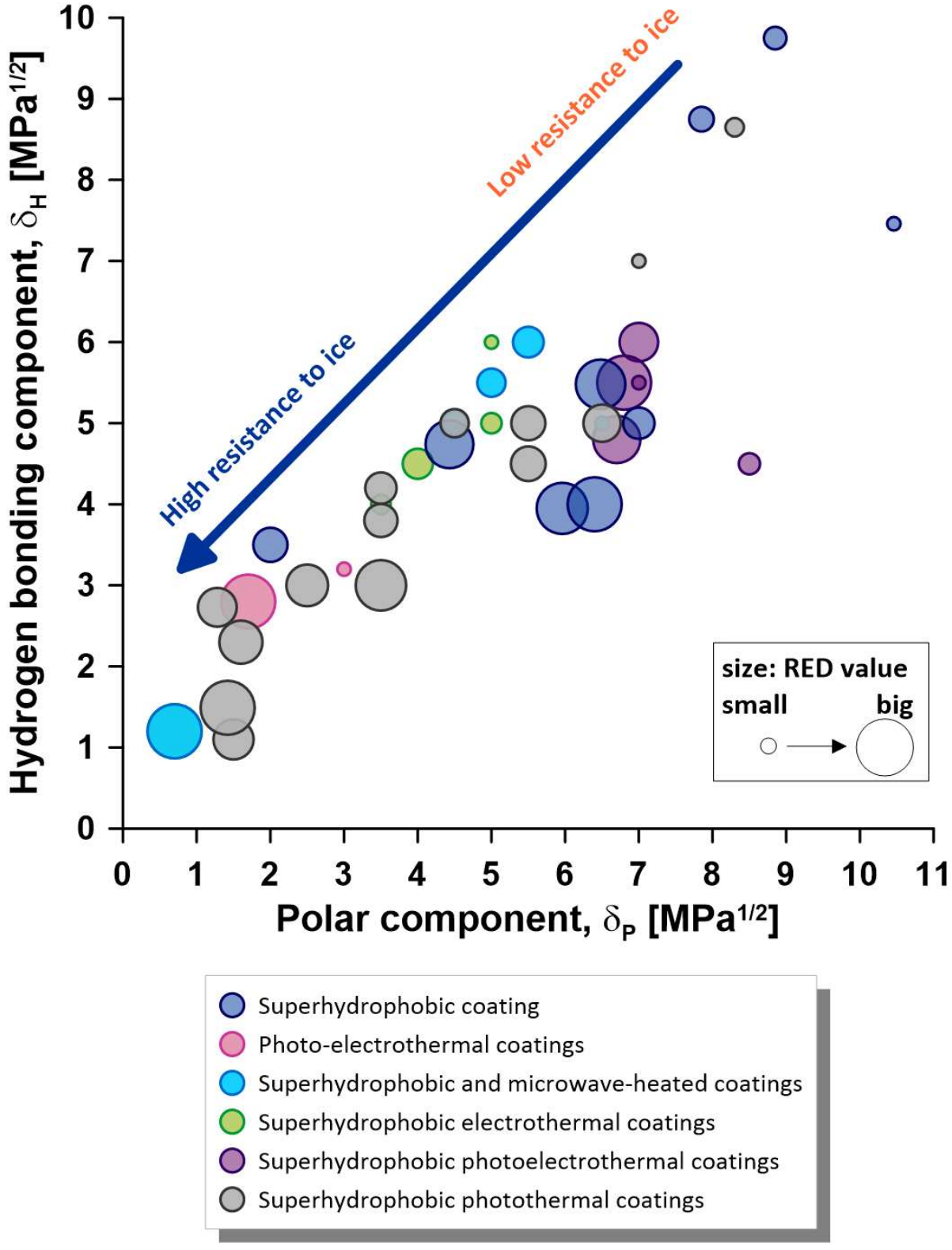

Fig. 19. Wettability *versus* ice resistance.

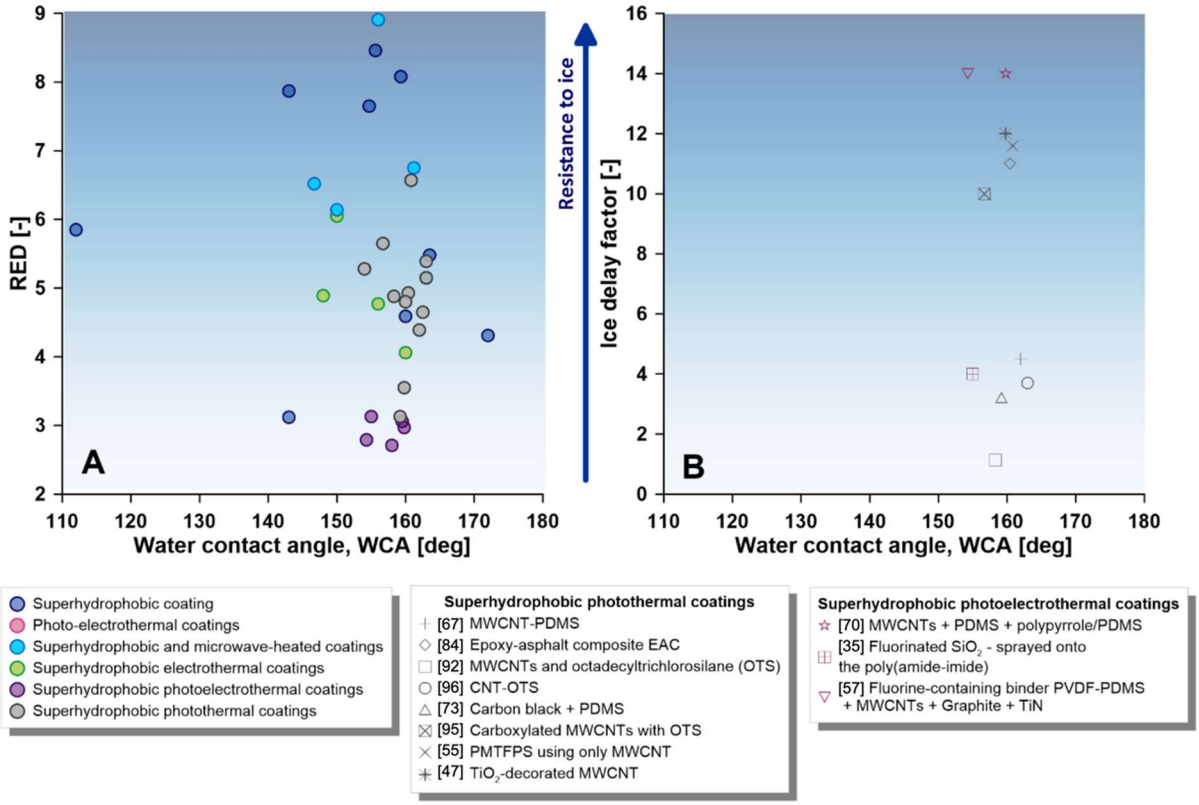

Fig. 20. Wettability and relative energy distance (RED) (A) and relation between wettability features and ice resistance (B).

Indeed, HSPs provide a scientifically robust framework for understanding and engineering the surface energy landscape of CNT-based anti-icing coatings. Through deliberate modulation of δ_d, δ_p, and δ_h, researchers can rationally design nanocomposite systems that achieve optimal dispersion, surface wettability, and interfacial thermal properties, leading to materials that exhibit significantly delayed ice nucleation, reduced adhesion, and improved de-icing efficiency under passive or active conditions.

Table 2. Values of HSP for the carbon-based anti-icing materials (CBAIMs) and interaction between CBAIMs and ice.

CNT/matrix	WCA [deg]	δ_D [MPa$^{1/2}$]	δ_P [MPa$^{1/2}$]	δ_H [MPa$^{1/2}$]	δ_{total} [MPa$^{1/2}$]	R_0	$\Delta_{CNT\text{-}ice}$ [MPa$^{1/2}$]	RED	Ref.
Superhydrophobic coating									
PDMS	112.0	15.50	2.00	3.50	16.02	7.50	43.90	5.85	[37]
MWCNTs (90 wt.%) and PDMS	159.3	18.83	5.96	3.95	20.14	5.25	42.41	8.08	[37]
MWCNTs + CNFs for CNT-CNF 1:1 – PM-MWCNT-CNF	160.0	19.9	7.85	8.75	23.11	8.15	37.41	4.59	[43]
SCF-MWCNT-CNF	172.0	19.4	8.85	9.75	23.45	8.40	36.17	4.31	[43]
MWCNT (1.25 wt.%) + polystyrene	143.0	18.65	10.46	7.46	22.64	12.20	38.07	3.12	[50]
MWCNT + TEOS	143.0	17.68	6.48	5.48	19.61	5.18	40.75	7.87	[56]
MWCNT + TEOS + SiO_2	154.7	17.05	4.43	4.74	18.24	5.49	41.99	7.65	[56]
PPFMCS composite	163.5	16.50	7.00	5.00	18.61	7.50	41.07	5.48	[81]
MWCNT xerogel	155.6	19.20	6.40	4.00	20.63	5.00	42.28	8.46	[87]
Photo-electrothermal coatings									
Dispersion of MWCNTs, graphite powder, and PDMS in the electrothermal layer	12.00*	17.20	1.70	2.80	17.51	6.80	44.67	6.57	[71]
CNTs dispersed in a PU matrix in the photothermal layer	82.9	16.30	3.00	3.20	16.88	6.74	43.87	6.51	[75]
Superhydrophobic and microwave-heated coatings									
CNTs + AMUS – amphiphilic copolymer with urea segment	161.2	17.00	5.50	6.00	18.85	6.00	40.48	6.75	[77]
CNTs + AMAC – amphiphilic copolymer with carbamate segment	146.7	17.20	5.00	5.50	18.74	6.30	41.10	6.52	[77]
CNTs + AMSC – amphiphilic copolymer with carbonate segment	150.0	17.50	4.50	5.00	18.75	6.80	41.72	6.14	[77]
CNT and hexadecyltrimethoxysilane (HDTMS)	156.0	16.30	0.70	1.20	16.36	5.22	46.50	8.91	[64]
MWCNTs covered with 1*H*,1*H*,2*H*,2*H*-perfluorodecyltrimethoxysilane – PC10 coating	163.0	15.80	6.50	5.00	17.80	8.00	41.18	5.15	[44]
Superhydrophobic electrothermal coatings									
Hierarchical graphene/CNT/SiO_2	160.0	18	5.00	6.00	19.62	10.00	40.64	4.06	[85]
Fluorinated MWCNTs mixed with epoxy resin – F-CNTs	148.0	16	5.00	5.00	17.49	8.50	41.57	4.89	[34]
Fluorinated MWCNTs mixed with epoxy resin – F-CEE	150.0	14.5	4.00	4.50	15.70	7.00	42.36	6.05	[34]
Epoxy/MWCNTs coating-epoxy/SiO_2/ hexadecyltrimethoxysilane (HDTMS) nanocomposite	156.0	16.30	0.70	1.20	16.36	5.22	46.50	8.91	[64]
MWCNT/Ferrite/Ni Chain/PDMS-coated cotton fabrics - MWCNT/CNF_3/Ni NC/PDMS	156.0	16.5	3.50	4.00	17.33	9.00	42.95	4.77	[72]
Superhydrophobic photothermal coatings									

PVDF + MWCNTs covered with 1*H*,1*H*,2*H*,2*H*-perfluorodecyltrimethoxysilane	163.0	15.80	6.50	5.00	17.80	8.00	41.18	5.15	[44]
MWCNT-PDMS	162.0	17	4.50	5.00	18.28	9.50	41.71	4.39	[67]
PDMS + CNTs + silicone resin		15.8	2.50	3.00	16.28	8.00	44.21	5.53	[29]
Epoxy-asphalt composite EAC	160.4	17	5.50	4.50	18.43	8.50	41.92	4.93	[84]
Fluorosilane + PU + CNT-based multilayer – CSPHC-3		16	3.50	3.00	16.65	7.00	43.91	6.27	[84]
MWCNTs and octadecyltrichlorosilane (OTS)	158.3	17.5	5.50	5.00	19.01	8.50	41.45	4.88	[92]
CNT-OTS adding ultrasonication to the preparation process	163.0	18	1.50	1.10	18.10	8.60	46.36	5.39	[96]
Carbon black + PDMS	159.2	18	7.00	7.00	20.54	12.50	39.16	3.13	[73]
Carboxylated MWCNTs with OTS	156.7	17.2	1.60	2.30	17.43	8.00	45.17	5.65	[95]
Dodecylamine connected to the CNT through pretreatment with dopamine hydrochloride	162.5	17.5	3.50	4.20	18.33	9.20	42.78	4.65	[45]
Papilla-like microstructure by adding polydopamine-coated layered	160.0	18.1	3.50	3.80	18.82	9.00	43.18	4.80	[46]
PMTFPS using only MWCNT	160.8	15.89	1.42	1.49	16.02	7.00	45.99	6.57	[55]
TiO_2-decorated MWCNT	159.8	17.15	8.30	8.65	20.92	10.50	37.23	3.55	[47]
Nano-MOF on the CNT modified with octanoic acid	154.0	16.41	1.28	2.73	16.68	8.50	44.86	5.28	[74]
Superhydrophobic photoelectrothermal coatings									
MWCNTs + PDMS, + polypyrrole/PDMS	159.8	17.00	7.00	6.00	19.34	13.50	40.10	2.97	[70]
fluorinated SiO_2 - sprayed onto the poly(amide-imide)	155.0	17.20	6.80	5.50	19.30	13.00	40.64	3.13	[35]
MWCNTs + rGO + hydrophobic surfactant cellulose 1-butylimidazolium bis(trifluoromethane)sulfonimide originating from natural cellulose	158.0	16.50	7.00	5.50	18.75	15.00	40.58	2.71	[86]
Fluorine-containing binder PVDF-PDMS in a coating composed of MWCNTs, graphite powder, and TiN	154.3	17.50	8.50	4.50	19.97	14.80	41.26	2.79	[57]
CNTs +G closed between two layers of PDMS, sprayed with a dispersion of SiO_2, TiN, and PDMS	159.5	17.20	6.70	4.80	19.07	13.50	41.34	3.06	[68]

*Sliding angle

9. Conclusions and perspectives

CNT-based coatings represent one of the most promising directions in developing advanced ice-repellent surfaces (**Table 3**). The combination of their high aspect ratio, mechanical strength, electrical and thermal conductivity, and chemical tunability enables the fabrication of

multifunctional coatings adaptable to various substrates and environmental conditions. This review outlines how CNTs were utilized across multiple anti-icing strategies, from passive superhydrophobic surfaces to active photothermal, electrothermal, and synergistic systems.

Overall, the data reflect a clear preference for passive and light-driven strategies, favoring simplicity, scalability, and energy efficiency. Superhydrophobic CNT-based coatings remain the most widely explored and industrially viable. The native roughness of CNT assemblies facilitates the creation of hierarchical surfaces. This property and combining with low-surface-energy compounds, especially PDMS, OTS, or fluorosilanes, is crucial for achieving contact angles above 150°. An emerging strategy for reducing the surface energy of CNTs is their hydrogenation, which may simplify coating composition without reducing effectiveness.

The scalability of CNT-based ice-repellent coatings is a key factor influencing the transition from laboratory prototypes to real-world applications. Coating techniques such as spray coating, dip coating, and blade scraping have already been demonstrated and are appropriate for the large-area deposition of CNT composites on various substrates. Further research may examine more roll-to-roll easy-to-scale techniques, such as flexography or rotary screen printing.

The economic aspects of CNT-based ice-phobic coatings are essential for their potential use in commercial and industrial settings. The cost of pristine CNTs remains relatively high due to the energy-consuming synthesis and purification. However, several examples from recent literature demonstrate that high-performance coatings can be achieved with low CNT content, especially when combined with cost-efficient polymers or powder fillers for passive protection methods.

Although CNTs may act as mechanical reinforcements within polymer matrices, long-term durability remains challenging. Surface functionalization and structural reinforcement of CNTs were presented as a solution to this problem. Hierarchical hybrids, such as CNT/SiO_2

composites or CNT/graphene hybrids, further reduce surface energy while improving mechanical integrity and surface roughness. Fluorinated CNTs, produced *via* plasma fluorination or chemical grafting of fluorinated moieties *via* nucleophilic substitution, would offer ultra-low surface energy and chemical stability. As an alternative, CNTs can be introduced in dynamic polymer systems, facilitating self-restoration of a damaged surface and ice-phobicity. These systems promise to extend coating lifetimes in harsh environments and should be the direction for further development.

CNT-based ice-prevention coatings show great potential in performance and functionality, but sustainability remains marginalized. Considering the numerous developed coatings, only a few discuss eliminating organic solvents, recyclability, or plant-originating raw materials. Furthermore, surface modifications using fluorinated compounds raise environmental concerns due to the persistence of perfluorinated residues and their potential toxicity.

It is also worth highlighting that there is a strong need for the standardization of measurements. A major challenge in evaluating and comparing CNT-based ice-phobic coatings lies in the paradox of abundance. Across the literature, various experimental setups, measured quantities, and measurement conditions are used to assess anti-icing or deicing performance, such as freezing delay time, melting time, frosting and defrosting time, and ice accumulation. While each method offers significant understanding into specific aspects of performance, the diversity of conditions, such as temperature, relative humidity, droplet size, substrate orientation, flow, or stable environment, makes direct comparison between studies unreliable. Establishing consistent, benchmarked protocols would facilitate the identification of truly superior material systems. Since we have experience in the measurements on the “cold plate”, and there are commercially available systems for measurement of anti-icing properties using this method, based on this review, as well as on the results obtained in the present study, we propose the following guidelines for cold plate–based experiments: measurement of the droplet height after crystallization (this provides a correction for vaporization, although it is unnecessary if both the ambient temperature and droplet volume are assumed to remain constant). Whenever possible, droplet temperature should be measured using a thermocouple. However, the extent to which the presence of a thermocouple affects the icing process within a droplet remains an open

question. We recommend using a droplet volume of 6 μL (deionized water with a resistivity not higher than 15 MΩ·cm), which minimizes the influence of gravity and impurities. The ambient temperature around the droplet should be constant (thermostated environment) at 20 °C, with relative humidity maintained between 40 and 60%, which is typical for laboratory conditions.

A particularly important factor affecting the process—and one that complicates the comparison of data from different laboratories—is the thickness of the film serving as the anti-icing material (see, for example, Fig. 14 in [https://doi.org/10.1016/j.cej.2024.148777]). It has been demonstrated that film thickness can strongly influence the kinetics of icing on the cold plate. Therefore, to improve comparability of laboratory results within experimental limitations, we recommend using an anti-icing film thickness of 500 μm.

We eventually show, for the first time, that HSPs can be scientifically correlated to de-icing time and ice formation delay, particularly through their influence on surface wetting, interfacial heat transfer, and molecular interactions at the solid–ice and solid–water interfaces (**Fig. 21**). The de-icing time and ice formation delay (freezing delay) of CNT-based coatings are determined by a complex interplay of thermophysical and interfacial phenomena, all of which are sensitive to the surface energy characteristics of the coating. These characteristics, in turn, are directly influenced by HSPs of the materials that constitute the surface layer.

In summary, CNTs constitute versatile nanofillers for fabricating robust, multifunctional surfaces and facilitate effective ice prevention and removal in various applications across diverse environments. As demonstrated, even though the field has been extensively researched, critical challenges remain before widespread industrial implementation can be achieved. These include the scalability of synthesis and integration methods, long-term durability under real-world conditions, cost-effectiveness, and regulatory considerations. Addressing these aspects will be essential to translate laboratory success into the commercially-viable solutions. With continued interdisciplinary innovation, CNT-based surfaces are poised to play a pivotal role in the next generation of smart anti-icing technologies.

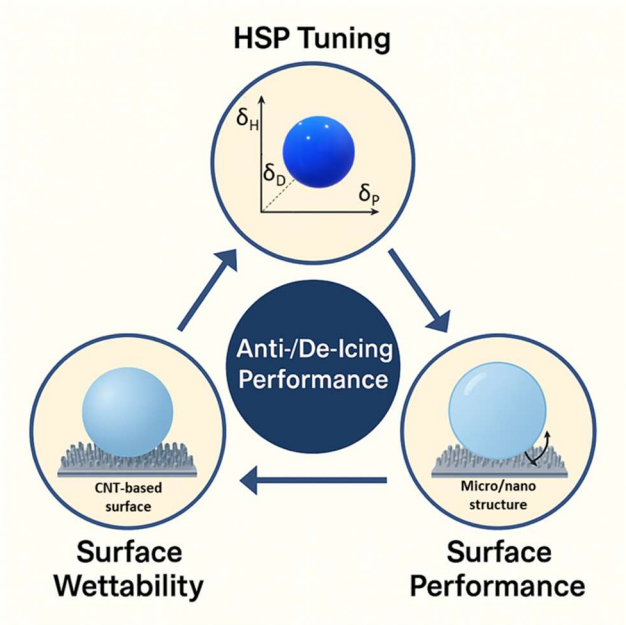

Fig. 21. Correlation of HSPs with anti-icing/de-icing performance.

Table 3. Chronologically sorted summary of reviewed research articles.

No.	Strategy of ice-prevention	Form of CNT	CNT modification	Additional substances	Binder	Preparation	Coating	Substrate	Effects	Potential application	Additional advantages	Ref.
1	superhydrophobic	pristine			silicone rubber	dispersion by ultrasonication	drop-casting	glass	55.4% less accumulated ice		mechanical durability, chemical resistance, thermal resistance, UV-light stability	[37]
2	electrothermal	pristine		non-commercial aqueous dispersion			rotary-screen printing	50% PET and 50% polyamide non-woven textile substrate	defrosting time: 25 min (3–4-mm-thick, –5° C, wind speed of 7 m s^{-1}, 70 V, 192 mA)	wind turbine blades		[93]
3	superhydrophobic, photothermal	modified	carboxylic, fluorinated with 1*H*,1*H*,2*H*,2*H*-perfluorodecyl-trimethoxysilane	silicon carbide	tetraethyl orthosilicate	dispersion by ultrasonication	spray-coating	'ethylene vinyl acetate'	4.4 times longer freezing time (–30° C, 30% RH); defrosting time: 250 s, (3-mm-thick, 808 nm, 1 W)			[42]
4	superhydrophobic	pristine			epoxy resin	dispersion by ultrasonication	spray-coating	Q235 carbon steel	no ice residue observed in the water dripping test		mechanical durability	[41]
5	superhydrophobic, lubricated	xerogel		perfluorodecalin		dispersion by ultrasonication	sprinkled on samples, pressed to each other, and milled in smooth movements to uniformity	steel covered with carbon adhesive tape	in the water dripping tests, the rate of ice formation remains several times lower than that of a sample without coating	wind turbine blades		[87]

6	superhydrophobic	modified	polystyrene grafted		PDMS; poly(ε-caprolactone)diol; dimer acid-glycerol modified polyol	simultaneous polymerization		glass and galvanized tin	9.6 times longer freezing time (–15° C)		mechanical durability, chemical resistance, self-cleaning properties, self-healing properties, thermal resistance	[50]
7	superhydrophobic	pristine		CNFs		supercritical fluid, physical mixing	drop-casting	fiber-reinforced polymer	no ice residue observed in the water dripping test		thermal stability, antifouling properties,	[43]
8	electrothermal	pristine		sodium dodecylbenzene sulfonate		dispersion by ultrasonication	spin-coating	glass	melting time: 56 s (–20° C, 50 V)	aircraft, radomes	transparency, radio-frequency transmittance	[4]
9	electrothermal	pristine		sodium dodecylbenzene sulfonate		dispersion by ultrasonication	spray-coating	glass	melting time: 350 s (–20° C, 40 V)	radomes	radio-frequency transmittance	[5]
10	amphiphobic, photothermal	modified	fluorinated		PU matrix	grinding	spray-coating	aluminum	15.8 times longer freezing time and 28.7 times longer freezing time under 1 sun illumination (–10° C)		self-cleaning properties, self-healing properties	[59]
11	superhydrophobic	pristine			acrylic acid		scrapping	glass, styrene-butadiene-styrene modified asphalt	1.2 times longer freezing time (–5° C)	asphalt pavement	anti-skid properties; prevention of water penetration into the pavement	[76]
12	superhydrophobic, electrothermal	modified	fluorinated with 1*H*,1*H*,2*H*,2*H*-perfluorooctyltri-ethoxysilane	graphene, silica nanoparticles		dispersion by ultrasonication and mechanical stirring	drop-casting	polycarbonate	5.9 times longer freezing time (–15° C, RH 30%); the ice (3-mm-thick) completely removed		mechanical durability, chemical resistance, thermal resistance	[85]

								within 70 s in glaze ice test (50 V, –5° C, RH 80%)			
13	electrothermal	pristine			PU matrix	dispersion by ultrasonication	spray-coating	glass fiber reinforced plastic coated with conductive silver adhesive	droplet department from angled surface in a 22.7% shorter time (–25° C, 0.5 W cm^{-2})	aircraft	suitable for curved and irregular surfaces	[52]
14	superhydrophobic, photothermal, electrothermal	pristine			fluorine-modified polyacrylate	grinding, mechanical stirring	spray-coating	glass	14 times longer freezing time (–15° C); no freeze under −30° C at 0.8 sun, or voltage to 10.5 V, melting times (−30° C): 14.3 min (1 sun), 3.1 min (12 V), 1.8 min (1 sun and 12 V)	solar battery	mechanical durability, self-cleaning properties	[60]
15	electrothermal	pristine			commercial ink Electra Colour™ – pristine Black	dispersion by ultrasonication	roll-to-roll slot-die coating	polyethylene terephthalate	an ice block melted in 3 min (–2° C, 40 V)	heaters	scalable method of coating	[88]
16	superhydrophobic, photothermal, electrothermal	modified	fluorinated	carbon powder	trifunctional poly(propylene glycol)	mechanical stirring	spray-coating	self-healable poly(urea–urethane)	melting time (–25° C, RH 30%): 148 s (15 V) and 265 s (1W, NIR) defrosting time (3 mm thick, –25° C, RH 80%): 530 s (15 V), 460 s (NIR), and 120 s (both)		mechanical, durability, self-healing properties	[54]

17	superhydrophobic, photothermal	modified	grafted with silica nanoparticles		epoxy resin	dispersion by ultrasonication and mechanical stirring	spray-coating	aluminum	11 times longer freezing time (–20° C); defrosting time (808 nm, –20° C, RH 70%): 60 s		mechanical durability	[63]
18	electrothermal	pristine			PU/ paraffin composite	dispersion by ultrasonication and mechanical stirring	spray-coating	glass fiber reinforced plastics	de-icing time (–25° C, 0.3 W cm^{-2}): 45 s			[51]
19	superhydrophobic	pristine		zinc oxide	PDMS	dispersion by ultrasonication	spray-coating	epoxy, silicone rubber, nylon, polymethyl methacrylate, PTFE, and insulating paper	2 times longer freezing time (–6° C)	outdoor insulators	high DC flashover strength, self-cleaning properties, good abrasive resistance, UV resistance	[38]
20	photothermal, lubricated	pristine		paraffin	PDMS	dispersion by ultrasonication	spin-coating	glass	about 10 times longer freezing time (–20° C, RH 80%); melting time 55 s	wind turbine blades		[39]
21	superhydrophobic, photothermal	pristine		1*H*,1*H*,2*H*,2*H*-perfluorodecyl-trimethoxysilane	PVDF	dispersion by ultrasonication	spray-coating	glass covered with silicone rubber	3,7 times longer freezing time (–20° C, RH 65%)		mechanical durability, chemical resistance	[44]
22	superhydrophobic, photothermal	modified	modified with dopamine and dodecylamine *via* Michael addition reaction		silicone resin	mechanical stirring	spray-coating	glass	3.3 times longer freezing time (–20° C, RH 35%); defrosting time (2 mm thick, 1 sun, –20° C, RH 35%): 423 s	Solar energy-facilitated materials	mechanical durability, chemical resistance, thermal resistance, self-cleaning properties, self-healing properties	[45]

23	superhydrophobic, photothermal	modified	Modified with PMTFPS		fluorinated silicone resin	grinding	using a coater	tin	11.6 times longer freezing time (–15° C), melting time (150 W): 90 s		mechanical durability, chemical resistance	[55]
24	electrothermal	modified	sulfonated, in ready aqueous paste	poly(3,4-ethylenedioxy-thiophene)			spray-coating	sandwich-structured glass fiber-reinforced polymer composite	3.4 times shorter melting time (7.44 W, 5-mm-thick, RT)	wind turbines	flexibility	[94]
25	superhydrophobic, microwave heating	pristine			commercial paint XS-B20 black acrylic road marking paint		sprinkled on uncured acrylic with an 800-mesh sieve	asphalt	1.6 times longer freezing time; 42.86% faster melting (10-mm-thick)	roads, pavements	load wheel rolling resistance	[77]
26	superhydrophobic, photothermal	modified	fluorinated with 1*H*,1*H*,2*H*,2*H*-perfluorodecyl-triethoxysilane	polydopamine-coated basic zinc acetate microparticles, 1*H*,1*H*,2*H*,2*H*-perfluorodecyl-triethoxysilane	aluminum phosphate binder	dispersion by ultrasonication	spray-coating	wood, PTFE, fiber-reinforced plastic, aluminum alloy, glass	freezing time 112.5 min (−10° C and RH 75%), melting time (−15 °C): 245 s (1 sun), 96 s (40 V); defrosting time (−15 °C): 510 s (1 sun), 22 s (40 V)			[46]
27	photothermal, lubricated	pristine		silicone oil	PDMS	mechanical stirring		glass, aluminum	9.6 times longer freezing time (–5° C) and 8.7 (–10° C); 25.8 times longer frosting time (–10° C, RH 40%); melting time (–10° C, 1 sun): 6 min			[53]

28	superhydrophobic, photothermal, electrothermal	pristine		reduced graphene oxide	cellulose 1-butylimidazolium bis(trifluoromethane)sulfonimide	dispersion by ultrasonication	spray-coating	glass	freezing time (–15° C): 7,200 s, 10,000 s (1 sun); melting time: 115 s (1 sun), 20 s (12 V)	wind turbine blades	mechanical durability	[86]
29	superhydrophobic, electrothermal	pristine			epoxy resin	mechanical stirring	brushing	glass	6.5 times longer freezing time (-15° C); melting time (-15° C, RH 30%): 78 s	wind turbine blades	mechanical durability, chemical resistance	[64]
30	superhydrophobic, photothermal	modified	grafted with silica nanoparticles	cetyltrimethylammonium bromide	epoxy resin	dispersion by ultrasonication and mechanical stirring	spray-coating	concrete	16 times longer freezing time (–10° C, RH 35%); melting time 535 s (–10° C, RH 35%, 1 kW m^{-2})	buildings	sustainability, mechanical durability	[30]
31	Photothermal	pristine			water-based polyacrylic resin, vinyl chloride resin	mechanical stirring and grinding	spray-coating and laser etching	aluminum	11.1 times longer freezing time (1 sun, –10° C); 12.3 times longer frosting time (1 sun, –10° C)			[32]
32	superhydrophobic, photothermal	modified	coated with silver		fluorine-containing polyacrylic emulsion	dispersion by ultrasonication and mechanical stirring, shaking	spray-coating	concrete	3.3 times longer freezing time (−20° C), 1.85 times shorter ice cube melting time (1 sun)	buildings	mechanical durability	[33]
33	superhydrophobic, photothermal	modified	functionalized with titanium dioxide		epoxy resin	dispersion by ultrasonication	spray-coating	epoxy resin	12.1 times longer freezing time (-15° C); 11.2 times shorter melting time (-20° C)		mechanical durability	[47]
34	photothermal, lubricated	modified	hydroxylated	paraffin wax		dispersion by ultrasonication	filtration under vacuum	cellulose acetate film	(−17° C, 1 sun) droplets did not freeze until complete evaporation;	underwater applications	self-healing properties, mechanical stability, harsh-condition	[40]

								11.9 times longer freezing time (−20° C, 1 sun)		resistance, chemical resistance	
35	superhydrophobic, electrothermal	modified	fluorinated		epoxy resin	mechanical stirring	spray-coating	glass	freezing time: 8 h (15 V, –20° C) and 4.2 h (10 V, –20° C)		mechanical durability, chemical resistance, thermal resistance	[34]
36	superhydrophobic, photothermal, electrothermal	pristine		fluorinated silica nanoparticles		dispersion by ultrasonication	spray-coating	glass covered with poly(amide imide)	4 times longer the freezing time (-20° C), melting time (-15° C): 500 s (36 V), 120 s (0.2 W cm^{-2})		flexibility, mechanical durability, chemical resistance, UV light stability, thermal resistance	[35]
37	superhydrophobic, photothermal	pristine		mesoporous silica	PDMS, polyamide resin, silicone resin	dispersion by ultrasonication	spray-coating	aluminum	73 times longer freezing time (–20° C); defrosting time (808 nm, 1.5 W cm^{-2}, –15° C, RH 50%): 480 s	rotor wings	mechanical durability, chemical resistance,	[29]
38	superhydrophobic, photothermal	pristine			PDMS, superhydrophobic commercial coating	mechanical stirring	molded and spray-coated with a superhydrophobic coating	concrete	12.6 times longer freezing time (–25° C), 0.54 times shorter melting time (NIR, 808 nm)	buildings	self-cleaning properties, chemical resistance, mechanical durability, thermal resistance	[67]
39	superhydrophobic, photothermal	modified	grafted with silica nanoparticles		PDMS	mechanical stirring	spray-coating	PU foam	melting time (–20° C, RH 40%, 1 kW m^{-2}): 13 min		mechanical durability	[48]

40	superhydrophobic, photothermal, electrothermal	modified	modified with cethytrimethylsiloxane		epoxy resin	dispersion by ultrasonication	spray-coating	glass	25.7 (–10° C), 18.5 (–15° C), 11.1 (–20° C) times longer freezing time; melting time (–15° C): 175 s (1.5 sun), 65 s (25 V); 7.9 times longer frosting time (–15° C), defrosting time (–15° C) 237 s (1.5 sun) 35 s (25 V) (RH 42%)	wind turbines	self-cleaning properties, chemical resistance, mechanical durability	[36]
41	superhydrophobic	modified	grafted with silica nanoparticles and dodecyltrimethoxysilane via sol-gel reaction		epoxy resin	dispersion by ultrasonication and mechanical stirring	spray-coating	asphalt	the bonding strength between the coated pavement and ice was 0.723 times that of direct ice pavement bonding strength	pavement	chemical resistance, skid resistance, mechanical durability, rutting resistance	[56]
42	photothermal	modified	carboxylated	silica aerogel, Triton X-100		dispersion by ultrasonication	spray-coating and brushing	glass	defrosting time (–4° C, 3-mm-thick): 230 s	wind turbines	chemical resistance, mechanical durability,	[89]
43	superhydrophobic, Photothermal, electrothermal	pristine		Graphene	PDMS	dispersion by ultrasonication	vacuum filtration, spray-coating	glass	3.1 longer freezing time (-20° C), 34.8 longer time without freezing (–20° C, 2 V or 1.8 V and 10.8 sun), defrosting time (–20° C): 128 s (2 V)		flexibility, mechanical durability	[68]

44	superhydrophobic, microwave heating	pristine		micro-sized iron powder	fluorinated silicone polymer, modified epoxy polyester	mechanical stirring	spray-coating	glass, asphalt	200 g ice cubes (–10° C), melting rate 8.37 g min^{-1} and an initial melting time of only ca. 30 s	pavements	mechanical durability, skid resistance	[78]
45	superhydrophobic, photothermal, electrothermal	pristine		graphite powder, titanium nitride	PDMS, PVDF	dispersion by ultrasonication and mechanical stirring	scraping	glass	14 times longer freezing time (–15° C, RH 65%); melting time (–15° C, RH 65%): 73 s and evaporation after 1200 s (0.5 sun, 0.28 W cm^{-2} electrothermal heating)		thermal resistance, self-cleaning properties	[57]
46	superhydrophobic, photothermal	modified	grafted with biochar nanoparticles		polyaspartic ester polyurea	mechanical stirring	spray-coating	epoxy resin	melting time 128 s, defrosting in 210 s (–10° C, RH 70%, 1 sun)		self-cleaning properties, mechanical durability, chemical resistance, from recycled crops, antifouling properties	[49]
47	superhydrophobic	pristine			PDMS	dispersion by ultrasonication and mechanical stirring	spray-coating	methyl vinyl silicone rubber	3.8 times longer freezing time (–20° C)	aerospace	self-cleaning properties, mechanical durability, chemical resistance	[69]
48	superhydrophobic, photothermal	modified	modified with octadecyl trichlorosilane		epoxy resin	dispersion by ultrasonication and mechanical stirring	spray-coating	concrete	12.4 times longer freezing time (–10° C)	pavement		[66]

49	superhydrophobic, photothermal	modified	modified with octadecyl trichlorosilane	*n*-tetradecane		mechanical stirring	spray-coating	concrete	9.8 times longer freezing time (−10° C); melting time: 173 s (1 sun)		mechanical durability, chemical resistance, thermal resistance, reduced water absorption	[95]
50	superhydrophobic, photothermal	modified	modified with PMTFPS		fluorinated silicone resin	grinding	applied with a controlled wet film thickness of 500 μm	tin	3.5 (–10° C) and 15 (–15° C) times longer freezing time; melting time: 10 s (150 W)		mechanical durability, thermal resistance, chemical resistance	[79]
51	Photothermal, lubricated	pristine		silicone oils	polysilazane	mechanical stirring	immersing	aluminum	4 times longer freezing time (–10° C), melting time: 83 s (10 sun)		chemical resistance, lubricant retention in air-blowing and shear-spinning test	[91]
52	superhydrophobic, photothermal, electrothermal	modified	covered with iron(III) oxide		PDMS	mechanical stirring	scrapping	silver electroless plated aramid paper	melting time: 210 s (0.1 W cm^{-2}), 180 s (1 sun)	EM devices, *e.g.*, signal stations, radar units	EMI shielding, self-cleaning properties, chemical resistance, thermal resistance	[58]
53	superhydrophobic, photothermal	pristine		silicon carbide		mechanical stirring	spray-coating	antifreeze protein modified emulsified asphalt	10.1 times longer freezing time (–8° C) and 11 times longer freezing time (1 kW m^{-2}); melting time (–12° C, 10 mm thick): 26 min (NIR, 2 kW m^{-2}), 11 min (NIR, 4 kW m^{-2})	pavements	mechanical durability, skid resistance	[84]

54	superhydrophobic, photothermal	pristine		PTFE	mechanical stirring	spray-coating	emulsified asphalt	2.4 times longer freezing time (–8° C); 2 times shorter melting time (–20° C, NIR)	roads	mechanical durability, skid resistance	[80]
55	hydrophobic	pristine		silicone rubber	mechanical stirring	spray-coating	glass, emulsified asphalt	1.7 times longer freezing time (–10° C)	roads	skid resistance, UV light resistance, reduced water absorption	[61]
56	superhydrophobic, photothermal, electrothermal	pristine		PDMS	dispersion by ultrasonication and mechanical stirring	spray-coating	aluminum covered with PDMS	14 times longer freezing time (–10° C); melting time (–10° C): 360 s (1 sun); defrosting time (–10° C): 60 s (1 sun), 120 s (0.2 W cm^{-2})		self-cleaning properties, mechanical durability, chemical resistance	[70]
57	superhydrophobic, photothermal	pristine	Octadecyl-trichlorosilane		mechanical stirring	spray-coating	copper	250 times (–10° C) and 103 times (–15° C) longer freezing time			[92]
58	superhydrophobic, photothermal	pristine		epoxidized soybean oil with specially synthesized curing agent (condensed vanillin and 1,10-diaminodecane)		spray-coating	glass, aluminum	9.4 times longer freezing time, 2 times shorter defrosting time (–20° C, 1.6 W cm^{-2}); 4.7 times shorter melting time (1.6 W/cm^{-2})		self-healing properties, recyclable, thermal resistance, UV light resistance, chemical resistance	[83]
59	superhydrophobic, photothermal	pristine	Octadecyl-trichlorosilane		mechanical stirring	spray-coating	copper	3.4 times and 4.7 times (1 sun) longer frosting time (–10° C) 1.9 times shorter defrosting time, 3.4 times			[96]

								shorter defrosting time (1 sun)			
60	photothermal, electrothermal, lubricated	pristine		graphite powder	PDMS	dispersion by ultrasonication and mechanical stirring	spray-coating	glass	4 times longer freezing time (−10° C); droplets not frozen after 1800 s (–20° C, 0.2 sun, 0.1 W cm^{-2}); melting time: 290 s (0.2 sun, 0.1 W cm^{-2})	self-healing properties, mechanical durability, anti-fouling properties	[71]
61	superhydrophobic	pristine		dual-sized silicon carbide particles, perfluorooctyl-triethoxysilane	epoxy resin, silicone rubber	mechanical stirring	spray-coating	aluminum, steel, paper, glass	3.8 times longer freezing time (–10° C, RH 35%); 1.3 times shorter defrosting time (2-mm-thick, xenon lamp)	mechanical resistance, chemical resistance, thermal resistance, self-cleaning properties	[62]
62	superhydrophobic	modified	grafted with silica, fluorinated with 1*H*,1*H*,2*H*,2*H*-heptadecafluorodecyltrimethoxysilane		PVDF, poly(vinyl acetate)	dispersion by ultrasonication	spray-coating	6061 aluminum alloy	13.8 times longer freezing time (–20° C)	marine equipment	chemical resistance, self-cleaning properties, mechanical durability, thermal resistance, drag reduction performance	[81]
63	photothermal, electrothermal, lubricated	pristine		coconut wax and coconut oil	PU matrix	dispersion by ultrasonication and mechanical stirring	by a coating machine	fiberglass cloth covered with copper foil	melting time: 60 s (–80° C, 1 sun, 4.1 V); defrosting time: 180 s (–80° C, 1 sun, 4.1 V)		flexibility, self-healing properties, self-cleaning properties, chemical resistance,	[75]
64	superhydrophobic, photothermal	modified	grafted with silica, covered	*n*-tetradecane	epoxy resin	dispersion by ultrasonication	spray-coating	concrete	14.4 times longer freezing time (–10° C, RH 70%), melting time: 543 s	buildings	chemical resistance, mechanical durability,	[65]

			with dodecyl-trimethoxysilane			and mechanical stirring			(1W/cm^2, NIR, -10° C, RH 70%)		reduced water absorption	
65	superhydrophobic, photothermal, electrothermal	pristine			thermoplastic elastomer	dispersion by ultrasonication	spray-coating	anisotropic porous wood (balsa)	1.8 times longer freezing time (−25 °C, RH 60-70%), melting time: 580 s (1 sun), 300 s (4 V)	wooden building roofs	energy storage capacity	[90]
66	superhydrophobic, electrothermal	pristine		Ferrite nanoparticles, nickel nanochains	PDMS		immersing	cotton	30 times shorter melting time (ice in a bottle, 6 V)	wearable technologies	self-cleaning properties, electromagnetic shielding, motion sensing, flexibility, emergency signaling, breathability, thermal stability	[72]
67	superhydrophobic, photothermal	pristine			fluorine-oligomers-modified epoxy resin	dispersion by ultrasonication and mechanical stirring	spray-coating	2024 aluminum alloy first covered with unmodified epoxy resin	59.4 times longer freezing time (–10° C); melting time 7 min (1 sun, –30° C)	aircraft	mechanical durability, chemical resistance, UV light resistance	[82]
68	superhydrophobic, photothermal	modified	modified with octadecyl trichlorosilane	carbon black	PDMS	dispersion by ultrasonication and mechanical stirring	spray-coating	concrete covered with epoxy resin	3.2 times longer freezing time (–15° C, RH 25%), melting time 176 s (NIR, 200 mW cm^{-2})	roads, bridges, dams	chemical resistance, mechanical durability	[73]
69	superhydrophobic, photothermal	modified	MOF/CNT hybrid particles		PDMS	growing MOFs on CNT and hydrophobizing with octanoic acid using 1-(3-dimethylamino-	spray-coating	glass	supercooled droplets (-40° C, RH 30%, 1 sun) evaporated fully before freezing (60 s)		self-healing properties, transparency	[74]

					propyl)-3-ethylcarbo-diimide hydrochloride as a coupling agent					
70	electrothermal	pristine	sodium dodecyl sulphate	PU matrix	dispersion by ultrasonication and mechanical stirring	spray-coating	glass fiber-reinforced plastic	freezing time: 60 s (–15° C, 30 m s^{-1} flow condition) deicing time: 22 s (–15° C, 30 m s^{-1} flow condition, 8.5-mm-thick, 1.8 W cm^{-2})	aircraft	[31]

Author contributions

A.P.T. and S.B. supervised the project. M.T. and S.B. built the framework and organized the Figures. M.T., J.K., A.P.T., and S.B. wrote the initial version of the manuscript. M.T. drafted all of the sections apart from 'Hansen Solubility Parameters' section written by J.K. and A.P.T. All authors made intellectual contributions, edited the manuscript, and crafted 'Conclusions and outlook' section. Also, all authors have provided feedback and contributed to the manuscript writing and have approved the final version of the paper. S.B. submitted the manuscript and was the lead contact.

Conflict of interest

The authors declare no conflict of interest.

Acknowledgments

The authors are very grateful for the financial support from the National Science Centre, Poland, grant No. 2021/43/B/ST5/00421 in the framework of the OPUS-22 program. M.T. and S.B. acknowledge the supporting actions from EU's Horizon 2020 ERA-Chair project ExCEED, grant agreement No. 952008.

References

1 Y. Shen, X. Wu, J. Tao, C. Zhu, Y. Lai and Z. Chen, *Progress in Materials Science*, 2019, **103**, 509–557.

2 S. Boncel, A. Kolanowska, A. W. Kuziel and I. Krzyżewska, *ACS Appl. Nano Mater.*, 2018, **1**, 6542–6555.

3 A. Cortés, A. Jiménez-Suárez, M. Campo, A. Ureña and S. G. Prolongo, *European Polymer Journal*, 2020, **141**, 110090.

4 J. Hong, J. H. Jung, S. Yong, Y. Kim, J. Park, S. J. Lee and J. Choi, *Journal of Materials Research and Technology*, 2020, **9**, 10854–10862.

5 J. H. Jung, J. Hong, Y. Kim, S.-M. Yong, J. Park and S. J. Lee, *Archives of Metallurgy and Materials*, 2020, **65**, 1011–1014.

6 R. Rekuviene, S. Saeidiharzand, L. Mažeika, V. Samaitis, A. Jankauskas, A. K. Sadaghiani, G. Gharib, Z. Muganlı and A. Koşar, *Applied Thermal Engineering*, 2024, **250**, 123474.

7 M. Mao, J. Wei, B. Li, L. Li, X. Huang and J. Zhang, *Nat Commun*, 2024, **15**, 9610.

8 A. Kenzhebayeva, B. Bakbolat, F. Sultanov, C. Daulbayev and Z. Mansurov, *Polymers*, 2021, **13**, 4149.

9 Z. Zhang, H. Zhang, S. Yue and W. Zeng, *Energies*, 2023, **16**, 601.

10 E. Korczeniewski, P. Bryk, E. Olewnik – Kruszkowska, P. Kowalczyk, A. Z. Wilczewska, K. H. Markiewicz, S. Boncel, S. Al-Gharabli, M. Sprynskyy, M. Świdziński, D. J. Smoliński, K. Fujisawa, T. Hayashi, P. Płóciennik, J. Kujawa and A. P. Terzyk, *Composites Part B: Engineering*, 2025, **295**, 112153.

11 E. Korczeniewski, P. Bryk, P. Kowalczyk, A. Z. Wilczewska, S. Boncel, R. Jędrysiak, M. Świdziński, S. Al-Gharabli, E. Olewnik-Kruszkowska, J. Kujawa and A. P. Terzyk, *Chemical Engineering Journal*, 2024, **482**, 148777.

12 J. Chen, K. Li, S. Wu, J. Liu, K. Liu and Q. Fan, *ACS Omega*, 2017, **2**, 2047–2054.

13 J. Kujawa, S. Al-Gharabli, E. Korczeniewski, P. Bryk, E. Olewnik-Kruszkowska, W. Kujawski and A. P. Terzyk, *Desalination*, 2024, **573**, 117227.

14 H. Wang, P. Cao, S. Xu, G. Cui, Z. Chen and Q. Yin, *Heliyon*, 2024, **10**, e32319.

15 Z. Amjad, A. P. Terzyk and S. Boncel, *Nanoscale*, 2024, **16**, 9197–9234.

16 E. Korczeniewski, P. Bryk, G. S. Szymański, P. Kowalczyk, M. Zięba, W. Zięba, M. Łępicka, K. J. Kurzydłowski, S. Boncel, S. Al-Gharabli, M. Świdziński, D. J. Smoliński, K. Kaneko, J. Kujawa and A. P. Terzyk, *Chemical Engineering Journal*, 2023, **462**, 142237.

17 M. Małecka, A. Ciach, A. P. Terzyk, J. Kujawa, E. Korczeniewski and S. Boncel, *Advances in Colloid and Interface Science*, 2024, **334**, 103311.

18 B. Jóźwiak, Ł. Scheller, H. F. Greer, K. Cwynar, K. Urbaniec, G. Dzido, J. Dziadosz, R. Jędrysiak, A. Kolanowska, A. Blacha, S. Boncel and M. Dzida, *Journal of Molecular Liquids*, 2023, **391**, 123329.

19 A. W. Kuziel, G. Dzido, R. Turczyn, R. G. Jędrysiak, A. Kolanowska, A. Tracz, W. Zięba, A. Cyganiuk, A. P. Terzyk and S. Boncel, *Journal of Energy Storage*, 2021, **36**, 102396.

20 A. Kolanowska, A. P. Herman, R. G. Jędrysiak and S. Boncel, *RSC Adv.*, 2021, **11**, 3020–3042.

21 A. Kolanowska, A. W. Kuziel, A. P. Herman, R. G. Jędrysiak, T. Giżewski and S. Boncel, *Progress in Organic Coatings*, 2019, **130**, 260–269.

22 A. P. Herman and S. Boncel, *RSC Adv.*, 2018, **8**, 30712–30716.

23 X. Chi, J. Zhang, J. P. Nshimiyimana, X. Hu, P. Wu, S. Liu, J. Liu, W. Chu and L. Sun, *RSC Adv.*, 2017, **7**, 48184–48188.

24 J. Li, J. Ling, L. Yan, Q. Wang, F. Zha and Z. Lei, *Surface and Coatings Technology*, 2014, **258**, 142–145.

25 C. H. Lau, R. Cervini, S. R. Clarke, M. G. Markovic, J. G. Matisons, S. C. Hawkins, C. P. Huynh and G. P. Simon, *J Nanopart Res*, 2008, **10**, 77–88.

26 A. Takakura, K. Beppu, T. Nishihara, A. Fukui, T. Kozeki, T. Namazu, Y. Miyauchi and K. Itami, *Nat Commun*, 2019, **10**, 3040.

27 H. Kim, M. Wang, S. K. Lee, J. Kang, J.-D. Nam, L. Ci and J. Suhr, *Sci Rep*, 2017, **7**, 9512.

28 A. B. Kaul, J. B. Coles, M. Eastwood, R. O. Green and P. R. Bandaru, *Small*, 2013, **9**, 1058–1065.

29 L. Deng, Z. Wang, Y. Niu, F. Luo and Q. Chen, *Composites Science and Technology*, 2024, **245**, 110347.

30 S. Li, Y. Li, Y. Tan, J. Li, D. Wang, D. Yuan and J. Zhang, *Sustainability*, 2023, **15**, 15865.

31 X. Zhou, Y. Shen, Z. Wang, J. Jiang, S. Liu, W. Liu and Y. Lin, *Applied Thermal Engineering*, 2025, **266**, 125704.

32 Z. Lin, C. Ma, Z. Ma, L. Gao, W. Chen and G. Chen, *Chemical Engineering Journal*, 2023, **466**, 143067.

33 X. Liu, S. Li, Y. Wu, T. Guo, J. Xie, J. Tao, L. Dong and Q. Ran, *ACS Appl. Mater. Interfaces*, 2023, **15**, 44305–44313.

34 Q. Wu, Z. Zhao, P. Li, X. Ren, X. Wang, F. Zhou and S. Wang, *Colloids and Surfaces A: Physicochemical and Engineering Aspects*, 2023, **666**, 131332.

35 C. Chang, I. Noh, N. Zhou, J. Jeon, Y. Wang, H. D. Kim, Q. Liu, H. Ohkita, X. Tao and B. Wang, *Surfaces and Interfaces*, 2024, **52**, 104879.

36 Y. Guo, H. Zhao, C. Zhang and G. Zhao, *Chemical Engineering Journal*, 2024, **497**, 154383.

37 Z. Mokarian, R. Rasuli and Y. Abedini, *Applied Surface Science*, 2016, **369**, 567–575.

38 M.-X. Zhu, H.-G. Song, J.-C. Li, J.-Y. Xue, Q.-C. Yu, J.-M. Chen and G.-J. Zhang, *Chemical Engineering Journal*, 2021, **404**, 126476.

39 J. He, H. Tian, K. Yang, J. Jie, B. Chen, Z. Shu, J. Bao and M. Pu, *International Journal of Photoenergy*, 2022, **2022**, 1–8.

40 S. Tan, X. Han, S. Cheng, P. Guo, X. Wang, P. Che, R. Jin, L. Jiang and L. Heng, *Macromol. Rapid Commun.*, 2023, **44**, 2200816.

41 F. Zhang, H. Qian, L. Wang, Z. Wang, C. Du, X. Li and D. Zhang, *Surface and Coatings Technology*, 2018, **341**, 15–23.

42 G. Jiang, L. Chen, S. Zhang and H. Huang, *ACS Appl. Mater. Interfaces*, 2018, **10**, 36505–36511.

43 S. Rajiv, S. Kumaran and M. Sathish, *J of Applied Polymer Sci*, 2019, **136**, 47059.

44 G. Jiang, Z. Liu and J. Hu, *Adv Materials Inter*, 2022, **9**, 2101704.

45 Y. Li, H. Li, J. Wu, X. Yang, X. Jia, J. Yang, D. Shao, L. Feng, S. Wang and H. Song, *Applied Surface Science*, 2022, **600**, 154177.

46 R. Zan, Y. Li, S. Tao, G. Li, R. Wu, D. Liu, D. Peng, Y. Liu and L. Fei, *Langmuir*, 2022, **38**, 13584–13593.

47 X. Liu, H. Liu, Y. Li, F. Teng and C. Liang, *Applied Surface Science*, 2023, **640**, 158318.

48 C. Guo, K. Liu, C. Ma, P. Sun and L. Liang, *Applied Thermal Engineering*, 2024, **236**, 121907.

49 Y. Lei, L. Hu, S. Du, D. Xu and J. Yang, *Coatings*, 2024, **14**, 838.

50 T. Ghosh and N. Karak, *Journal of Colloid and Interface Science*, 2019, **540**, 247–257.

51 Z. Zhao, H. Chen, X. Liu, Z. Wang, Y. Zhu and Y. Zhou, *Cold Regions Science and Technology*, 2021, **184**, 103234.

52 Z. Zhao, H. Chen, X. Liu, Z. Wang, Y. Zhu and Y. Zhou, *Surface and Coatings Technology*, 2020, **404**, 126489.

53 L. Zhou, A. Liu, L. Zhou, Y. Li, J. Kang, J. Tang, Y. Han and H. Liu, *ACS Appl. Mater. Interfaces*, 2022, **14**, 8537–8548.

54 P. Wang, J. Wang, W. Duan, C. Li, H. Han and Q. Xie, *J Bionic Eng*, 2021, **18**, 1147–1156.

55 Y. Liu, Y. Shao, Y. Wang and J. Wang, *Colloids and Surfaces A: Physicochemical and Engineering Aspects*, 2022, **648**, 129335.

56 Z. He, H. Xu, Y. Zhou and Y. Tan, *Construction and Building Materials*, 2024, **441**, 137587.

57 L. Jiang, J. Sun, Y. Lin, M. Gong, K. Tu, Y. Chen, T. Xiao, P. Xiang and X. Tan, *Surface and Coatings Technology*, 2024, **476**, 130273.

58 J. Mei, H. Liao, M. Hou and J. Wang, *Colloids and Surfaces A: Physicochemical and Engineering Aspects*, 2024, **682**, 132885.

59 Y. Liu, Y. Wu, Y. Liu, R. Xu, S. Liu and F. Zhou, *ACS Appl. Mater. Interfaces*, 2020, **12**, 46981–46990.

60 Y. Liu, R. Xu, N. Luo, Y. Liu, Y. Wu, B. Yu, S. Liu and F. Zhou, *Adv Materials Technologies*, 2021, **6**, 2100371.

61 C. Peng, H. Yang, Z. You, L. Zhou, L. Bao, H. Liu, T. Wu, N. Zhao and F. Yang, *Progress in Organic Coatings*, 2024, **196**, 108736.

62 Z. Y. Xue, C. Q. Li, H. W. Niu, J. F. Ou, F. J. Wang, X. Z. Fang, W. Li and A. Amirfazl, *DJNB*, 2024, **19**, 383–400.

63 F. Zhang, D. Xu, D. Zhang, L. Ma, J. Wang, Y. Huang, M. Chen, H. Qian and X. Li, *Chemical Engineering Journal*, 2021, **423**, 130238.

64 J. Fan, Z. Long, J. Wu, P. Gao, Y. Wu, P. Si and D. Zhang, *J Coat Technol Res*, 2023, **20**, 1557–1568.

65 S. Li, X. Liu, C. Xing, Y. Tan, A. Xiao, Y. Wei, C. Li and M. Dai, *Journal of Building Engineering*, 2025, **105**, 112449.

66 S. Li, Y. Tan, M. Han, S. Xiao, S. Li and M. Dai, *Materials Letters*, 2024, **355**, 135463.

67 Z. Gu, M. Zhao, Q. Liu, C. Mao, L. Zhang, X. Sun and S. Lv, *Materials Today Communications*, 2024, **41**, 110623.

68 J. Huang, Z. Peng, B. Zhang, Y. Yao and S. Chen, *ACS Appl. Mater. Interfaces*, 2024, **16**, 44210–44224.

69 P. Li, Y. Xu, F. Zhang, S. Ren, B. Shi, M. Ning, H. Ma, J. Li and W. Sun, *Colloids and Surfaces A: Physicochemical and Engineering Aspects*, 2024, **694**, 134155.

70 S. Peng, X. Xiao, J. Wei and J. Wang, *Solar Energy*, 2024, **270**, 112384.

71 X. Xiao, F. Yao, M. Huang, J. Wei and J. Wang, *Langmuir*, 2024, **40**, 17151–17159.

72 T. Suryaprabha, S. Hong, T. Pham, M.-Y. Seo, T.-W. Kim and B. Hwang, *Chemical Engineering Journal*, 2025, **507**, 160378.

73 N. Zhang, X. Kong, Y. Chang, W. Qiao, M. Zhang and R. Kang, *Journal of Building Engineering*, 2025, **101**, 111842.

74 J. Zhang, V. Singh, P. Kabi, W. Huang, S. Bahal, I. Papakonstantinou and M. K. Tiwari, *Nano Today*, 2025, **62**, 102673.

75 Z. Chai, Z. Teng, P. Guo, Y. He, D. Zhao, X. Zuo, K. Liu, L. Jiang and L. Heng, *Small Methods*, 2025, **9**, 2400859.

76 C. Peng, X. Hu, Z. You, F. Xu, G. Jiang, H. Ouyang, C. Guo, H. Ma, L. Lu and J. Dai, *Construction and Building Materials*, 2020, **264**, 120702.

77 C. Peng, Y. Hu, Z. You, H. Yang, Y. Nie, T. Wu, H. Yang and R. Ou, *Construction and Building Materials*, 2022, **344**, 128289.

78 W. Jia, B. Ma, Q. Yang, P. Sun and X. Yang, *Construction and Building Materials*, 2024, **451**, 138868.

79 Y. Liu, Y. Shao, Y. Wang and J. Wang, *Adv Eng Mater*, 2024, **26**, 2300188.

80 C. Peng, D. Yang, Z. You, D. Ruan, P. Guan, Z. Ye, Y. Ning, N. Zhao and F. Yang, *Construction and Building Materials*, 2024, **416**, 135148.

81 P. Zhang, Y. Zhao, X. Gu, K. Yang, X. Zhang, M. Liu, M. Zhao and Y. Che, *Composites Science and Technology*, 2024, **257**, 110798.

82 L. Yang, Y. Li, D. Huan and C. Zhu, *Colloids and Surfaces A: Physicochemical and Engineering Aspects*, 2025, **709**, 136150.

83 X. Wang, X. Huang, Z. Ji, H. Sheng and H. Liu, *ACS Sustainable Chem. Eng.*, 2024, **12**, 7147–7157.

84 C. Peng, D. Yang, Z. You, D. Ruan, P. Guan, Z. Ye, Y. Ning, N. Zhao and F. Yang, *ACS Appl. Mater. Interfaces*, 2024, **16**, 35588–35603.

85 P. Wang, T. Yao, Z. Li, W. Wei, Q. Xie, W. Duan and H. Han, *Composites Science and Technology*, 2020, **198**, 108307.

86 Y. Cheng, Y. Wang, X. Zhang, J. Zhang, Z. He, J. Wang and J. Zhang, *Nano Res.*, 2023, **16**, 7171–7179.

87 M. Eseev, A. Goshev, S. Kapustin and Y. Tsykareva, *Nanomaterials*, 2019, **9**, 1584.

88 T. Rashid, H.-L. Liang, M. Taimur, N. Chiodarelli, H. A. Khawaja, K. Edvardsen and M. De Volder, *Cold Regions Science and Technology*, 2021, **182**, 103210.

89 J. He, J. Yan, M. Pu, J. Jie, G. Luo, Z. Zeng, Z. Duan and C. Huang, *J Coat Technol Res*, 2024, **21**, 1499–1512.

90 S. Sheng, Z. Zhang, Z. Zhao, Y. Ning, C. Yu, K. Liu and L. Jiang, *Adv Funct Materials*, 2025, 2424897.

91 J. Ma and J. Song, *Journal of Colloid and Interface Science*, 2024, **653**, 1548–1556.

92 W. Sun, Y. Wei, Y. Feng and F. Chu, *Energy*, 2024, **286**, 129656.

93 T. Fischer, J. Rühling, N. Wetzold, T. Zillger, T. Weissbach, T. Göschel, M. Würfel, A. Hübler and L. Kroll, *J of Applied Polymer Sci*, 2018, **135**, 45950.

94 G. Monastyreckis, J. T. Siles, P. Knotek, M. Omastova, A. Aniskevich and D. Zeleniakiene, *Materials*, 2022, **15**, 3535.

95 S. Li, Y. Tan, S. Li and A. Xiao, *Polymer International*, 2024, pi.6706.

96 Y. Wei, S. Gao, W. Sun, X. Wu, Y. Feng and F. Chu, *Applied Thermal Engineering*, 2024, **236**, 121876.